ISSN
2395-6992

International Journal of Engineering Research & Science

www.ijoer.com
www.adpublications.org

Volume-8! Issue-11! November, 2022 www.ijoer.com ! info@ijoer.com

Preface

We would like to present, with great pleasure, the inaugural volume-8, Issue-11, November 2022, of a scholarly journal, *International Journal of Engineering Research & Science*. This journal is part of the AD Publications series *in the field of Engineering, Mathematics, Physics, Chemistry and science Research Development*, and is devoted to the gamut of Engineering and Science issues, from theoretical aspects to application-dependent studies and the validation of emerging technologies.

This journal was envisioned and founded to represent the growing needs of Engineering and Science as an emerging and increasingly vital field, now widely recognized as an integral part of scientific and technical investigations. Its mission is to become a voice of the Engineering and Science community, addressing researchers and practitioners in below areas

Chemical Engineering	
Biomolecular Engineering	Materials Engineering
Molecular Engineering	Process Engineering
Corrosion Engineering	
Civil Engineering	
Environmental Engineering	Geotechnical Engineering
Structural Engineering	Mining Engineering
Transport Engineering	Water resources Engineering
Electrical Engineering	
Power System Engineering	Optical Engineering
Mechanical Engineering	
Acoustical Engineering	Manufacturing Engineering
Optomechanical Engineering	Thermal Engineering
Power plant Engineering	Energy Engineering
Sports Engineering	Vehicle Engineering
Software Engineering	
Computer-aided Engineering	Cryptographic Engineering
Teletraffic Engineering	Web Engineering
System Engineering	
Mathematics	
Arithmetic	Algebra
Number theory	Field theory and polynomials
Analysis	Combinatorics
Geometry and topology	Topology
Probability and Statistics	Computational Science
Physical Science	Operational Research
Physics	
Nuclear and particle physics	Atomic, molecular, and optical physics
Condensed matter physics	Astrophysics
Applied Physics	Modern physics
Philosophy	Core theories

Chemistry	
Analytical chemistry	Biochemistry
Inorganic chemistry	Materials chemistry
Neurochemistry	Nuclear chemistry
Organic chemistry	Physical chemistry
Other Engineering Areas	
Aerospace Engineering	Agricultural Engineering
Applied Engineering	Biomedical Engineering
Biological Engineering	Building services Engineering
Energy Engineering	Railway Engineering
Industrial Engineering	Mechatronics Engineering
Management Engineering	Military Engineering
Petroleum Engineering	Nuclear Engineering
Textile Engineering	Nano Engineering
Algorithm and Computational Complexity	Artificial Intelligence
Electronics & Communication Engineering	Image Processing
Information Retrieval	Low Power VLSI Design
Neural Networks	Plastic Engineering

Each article in this issue provides an example of a concrete industrial application or a case study of the presented methodology to amplify the impact of the contribution. We are very thankful to everybody within that community who supported the idea of creating a new Research with IJOER. We are certain that this issue will be followed by many others, reporting new developments in the Engineering and Science field. This issue would not have been possible without the great support of the Reviewer, Editorial Board members and also with our Advisory Board Members, and we would like to express our sincere thanks to all of them. We would also like to express our gratitude to the editorial staff of AD Publications, who supported us at every stage of the project. It is our hope that this fine collection of articles will be a valuable resource for *IJOER* readers and will stimulate further research into the vibrant area of Engineering and Science Research.

Mukesh Arora

(Chief Editor)

Board Members

Dr. M. Varatha Vijayan

Annauniversity Rank Holder, Commissioned Officer Indian Navy, Ncc Navy Officer (Ex-Serviceman Navy), Best Researcher Awardee, Best Publication Awardee, Tamilnadu Best Innovation & Social Service Awardee From Lions Club.

Dr. Mohamed Abdel Fatah Ashabrawy Moustafa

PhD. in Computer Science - Faculty of Science - Suez Canal University University, 2010, Egypt.

Assistant Professor Computer Science, Prince Sattam bin AbdulAziz University ALkharj, KSA.

Prof.S.Balamurugan

Dr S. Balamurugan is the Head of Research and Development, Quants IS & CS, India. He has authored/co-authored 35 books, 200+ publications in various international journals and conferences and 6 patents to his credit. He was awarded with Three Post-Doctoral Degrees - Doctor of Science (D.Sc.) degree and Two Doctor of Letters (D.Litt) degrees for his significant contribution to research and development in Engineering.

Dr. Mahdi Hosseini

Dr. Mahdi did his Pre-University (12^{th}) in Mathematical Science. Later he received his Bachelor of Engineering with Distinction in Civil Engineering and later he Received both M.Tech. and Ph.D. Degree in Structural Engineering with Grade "A" First Class with Distinction.

Dr. Anil Lamba

Practice Head – Cyber Security, EXL Services Inc., New Jersey USA.

Dr. Anil Lamba is a researcher, an innovator, and an influencer with proven success in spearheading Strategic Information Security Initiatives and Large-scale IT Infrastructure projects across industry verticals. He has helped bring about a profound shift in cybersecurity defense. Throughout his career, he has parlayed his extensive background in security and a deep knowledge to help organizations build and implement strategic cybersecurity solutions. His published researches and conference papers has led to many thought provoking examples for augmenting better security.

Dr. Ali İhsan KAYA

Currently working as Associate Professor in Mehmet Akif Ersoy University, Turkey.

Research Area: Civil Engineering - Building Material - Insulation Materials Applications, Chemistry - Physical Chemistry – Composites.

Dr. Parsa Heydarpour

Ph.D. in Structural Engineering from George Washington University (Jan 2018), GPA=4.00.

Dr. Heba Mahmoud Mohamed Afify

Ph.D degree of philosophy in Biomedical Engineering, Cairo University, Egypt worked as Assistant Professor at MTI University.

Dr. Aurora Angela Pisano

Ph.D. in Civil Engineering, Currently Serving as Associate Professor of Solid and Structural Mechanics (scientific discipline area nationally denoted as ICAR/08"–"Scienza delle Costruzioni"), University Mediterranea of Reggio Calabria, Italy.

Dr. Faizullah Mahar

Associate Professor in Department of Electrical Engineering, Balochistan University Engineering & Technology Khuzdar. He is PhD (Electronic Engineering) from IQRA University, Defense View, Karachi, Pakistan.

Prof. Viviane Barrozo da Silva

Graduated in Physics from the Federal University of Paraná (1997), graduated in Electrical Engineering from the Federal University of Rio Grande do Sul - UFRGS (2008), and master's degree in Physics from the Federal University of Rio Grande do Sul (2001).

Dr. S. Kannadhasan

Ph.D (Smart Antennas), M.E (Communication Systems), M.B.A (Human Resources).

Dr. Christo Ananth

Ph.D. Co-operative Networks, M.E. Applied Electronics, B.E Electronics & Communication Engineering Working as Associate Professor, Lecturer and Faculty Advisor/ Department of Electronics & Communication Engineering in Francis Xavier Engineering College, Tirunelveli.

Dr. S.R.Boselin Prabhu

Ph.D, Wireless Sensor Networks, M.E. Network Engineering, Excellent Professional Achievement Award Winner from Society of Professional Engineers Biography Included in Marquis Who's Who in the World (Academic Year 2015 and 2016). Currently Serving as Assistant Professor in the department of ECE in SVS College of Engineering, Coimbatore.

Dr. PAUL P MATHAI

Dr. Paul P Mathai received his Bachelor's degree in Computer Science and Engineering from University of Madras, India. Then he obtained his Master's degree in Computer and Information Technology from Manonmanium Sundaranar University, India. In 2018, he received his Doctor of Philosophy in Computer Science and Engineering from Noorul Islam Centre for Higher Education, Kanyakumari, India.

Dr. M. Ramesh Kumar

Ph.D (Computer Science and Engineering), M.E (Computer Science and Engineering).

Currently working as Associate Professor in VSB College of Engineering Technical Campus, Coimbatore.

Dr. Maheshwar Shrestha

Postdoctoral Research Fellow in DEPT. OF ELE ENGG & COMP SCI, SDSU, Brookings, SD Ph.D, M.Sc. in Electrical Engineering from SOUTH DAKOTA STATE UNIVERSITY, Brookings, SD.

Dr. D. Amaranatha Reddy

Ph.D. (Postdocteral Fellow, Pusan National University, South Korea), M.Sc., B.Sc. : Physics.

Dr. Dibya Prakash Rai

Post Doctoral Fellow (PDF), M.Sc., B.Sc., Working as Assistant Professor in Department of Physics in Pachhuncga University College, Mizoram, India.

Dr. Pankaj Kumar Pal

Ph.D R/S, ECE Deptt., IIT-Roorkee.

Dr. P. Thangam

PhD in Information & Communication Engineering, ME (CSE), BE (Computer Hardware & Software), currently serving as Associate Professor in the Department of Computer Science and Engineering of Coimbatore Institute of Engineering and Technology.

Dr. Pradeep K. Sharma

PhD., M.Phil, M.Sc, B.Sc, in Physics, MBA in System Management, Presently working as Provost and Associate Professor & Head of Department for Physics in University of Engineering & Management, Jaipur.

Dr. R. Devi Priya

Ph.D (CSE), Anna University Chennai in 2013, M.E, B.E (CSE) from Kongu Engineering College, currently working in the Department of Computer Science and Engineering in Kongu Engineering College, Tamil Nadu, India.

Dr. Sandeep

Post-doctoral fellow, Principal Investigator, Young Scientist Scheme Project (DST-SERB), Department of Physics, Mizoram University, Aizawl Mizoram, India- 796001.

Dr. Roberto Volpe

Faculty of Engineering and Architecture, Università degli Studi di Enna "Kore", Cittadella Universitaria, 94100 – Enna (IT).

Dr. S. Kannadhasan

Ph.D (Smart Antennas), M.E (Communication Systems), M.B.A (Human Resources).

Research Area: Engineering Physics, Electromagnetic Field Theory, Electronic Material and Processes, Wireless Communications.

Mr. Amit Kumar

Amit Kumar is associated as a Researcher with the Department of Computer Science, College of Information Science and Technology, Nanjing Forestry University, Nanjing, China since 2009. He is working as a State Representative (HP), Spoken Tutorial Project, IIT Bombay promoting and integrating ICT in Literacy through Free and Open Source Software under National Mission on Education through ICT (NMEICT) of MHRD, Govt. of India; in the state of Himachal Pradesh, India.

Mr. Tanvir Singh

Tanvir Singh is acting as Outreach Officer (Punjab and J&K) for MHRD Govt. of India Project: Spoken Tutorial - IIT Bombay fostering IT Literacy through Open Source Technology under National Mission on Education through ICT (NMEICT). He is also acting as Research Associate since 2010 with Nanjing Forestry University, Nanjing, Jiangsu, China in the field of Social and Environmental Sustainability.

Mr. Abilash

MTech in VLSI, BTech in Electronics & Telecommunication engineering through A.M.I.E.T.E from Central Electronics Engineering Research Institute (C.E.E.R.I) Pilani, Industrial Electronics from ATI-EPI Hyderabad, IEEE course in Mechatronics, CSHAM from Birla Institute Of Professional Studies.

Mr. Varun Shukla

M.Tech in ECE from RGPV (Awarded with silver Medal By President of India), Assistant Professor, Dept. of ECE, PSIT, Kanpur.

Mr. Shrikant Harle

Presently working as a Assistant Professor in Civil Engineering field of Prof. Ram Meghe College of Engineering and Management, Amravati. He was Senior Design Engineer (Larsen & Toubro Limited, India).

Zairi Ismael Rizman

Senior Lecturer, Faculty of Electrical Engineering, Universiti Teknologi MARA (UiTM) (Terengganu) Malaysia Master (Science) in Microelectronics (2005), Universiti Kebangsaan Malaysia (UKM), Malaysia. Bachelor (Hons.) and Diploma in Electrical Engineering (Communication) (2002), UiTM Shah Alam, Malaysia.

Mr. Ronak

Qualification: M.Tech. in Mechanical Engineering (CAD/CAM), B.E.

Presently working as a Assistant Professor in Mechanical Engineering in ITM Vocational University, Vadodara. Mr. Ronak also worked as Design Engineer at Finstern Engineering Private Limited, Makarpura, Vadodara.

Table of Contents

Volume-8, Issue-11, November 2022

Indoor Environment of Buildings – Quality and Basic Ventilation Air Parameters: Part II

Ľubomíra Kmeťová[1*], Filip Duda[2], Lukáš Tóth[3]

Department of Power Engineering, Faculty of Mechanical Engineering, Technical University of Košice, Slovakia
*Corresponding Author

Received: 10 October 2022/ Revised: 24 October 2022/ Accepted: 10 November 2022/ Published: 30-11-2022

Abstract**—** *A series of articles focused on the indoor environment of buildings. Articles discuss the importance of a quality indoor environment and the implementation of the measurement of the parameters of the outgoing air from the indoor environment in the ventilation shaft of a panel house. The content of the second article is the determination of the procedure for measuring the speed, temperature and humidity of the air flowing through the ventilation shaft at the exit from the air duct of the selected panel house.*

Keywords**—** ***Air Flow Rate, Air Temperature, Measurement of Air Parameters, Relative Air Humidity, Ventilation Shaft.***

I. INTRODUCTION

Following the article Part I., the second article is devoted to the monitoring of the internal environment of living spaces. Article Part II. maps the procedure of measuring the ventilation air parameters of living spaces, specifically an 8-storey panel house in Slovakia. The methodology for measuring the quantity and parameters of the ventilation air in the selected panel house consists of several points (Fig. 1):

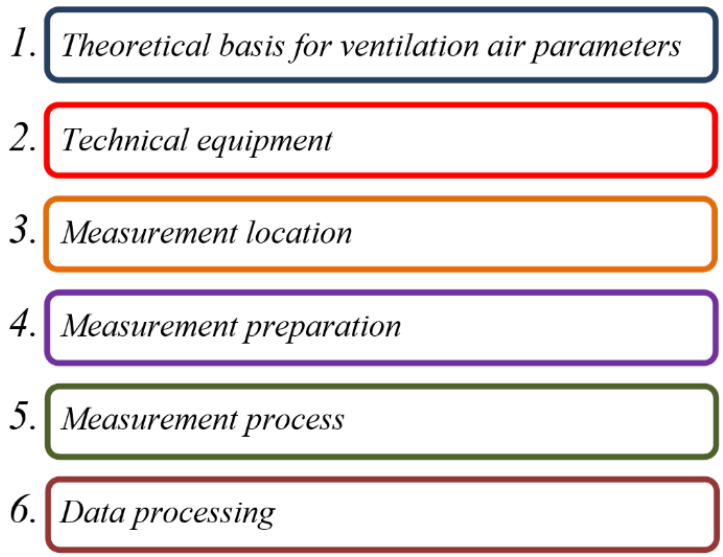

FIGURE 1: The methodology for measuring the quantity and parameters of the ventilation air

II. THEORETICAL BASIS FOR VENTILATION AIR PARAMETERS

The theoretical basis for ventilation air parameters was described in the first article Indoor Environment of Buildings – Quality and Basic Ventilation Air Parameters, Part I.. To determine the quantity of air that leaves the air duct, it is necessary to measure the following air parameters at the outlet of the air duct:

a) air flow velocity,

b) air temperature,

c) air humidity.

III. TECHNICAL EQUIPMENT

The measurement of the air parameters was performed using the measuring and recording devices shown in Table 1.

TABLE 1

TECHNICAL EQUIPMENT[1]

Type of measuring equipment	Producer	Measured parameter
Propeller probe FV A915-S140 	AHLBORN	Air velocity in the air duct
Combined temperature and humidity sensor FH A646 	AHLBORN	Air temperature in the duct
		Relative air humidity in the duct
Data logger ALMEMO 2390-8 	AHLBORN	Recording of measured data

IV. MEASUREMENT LOCATION

An apartment building of type T 08B KE (Fig. 2) located in Slovakia at an altitude of 206 m above sea level was chosen for the measurement of ventilation air parameters in the ventilation shaft of the panel house.

FIGURE 2: Schematic illustration of terraced panel house type T 08 B KE[2]

The selected panel house is a terraced building with 8 residential floors. Each floor of the subject panel house (Fig. 3) consists of two 3-room and one 1-room apartment. Each of the apartments has its own installation shaft, which includes an air duct – one pipe is common to 8 apartments [2].

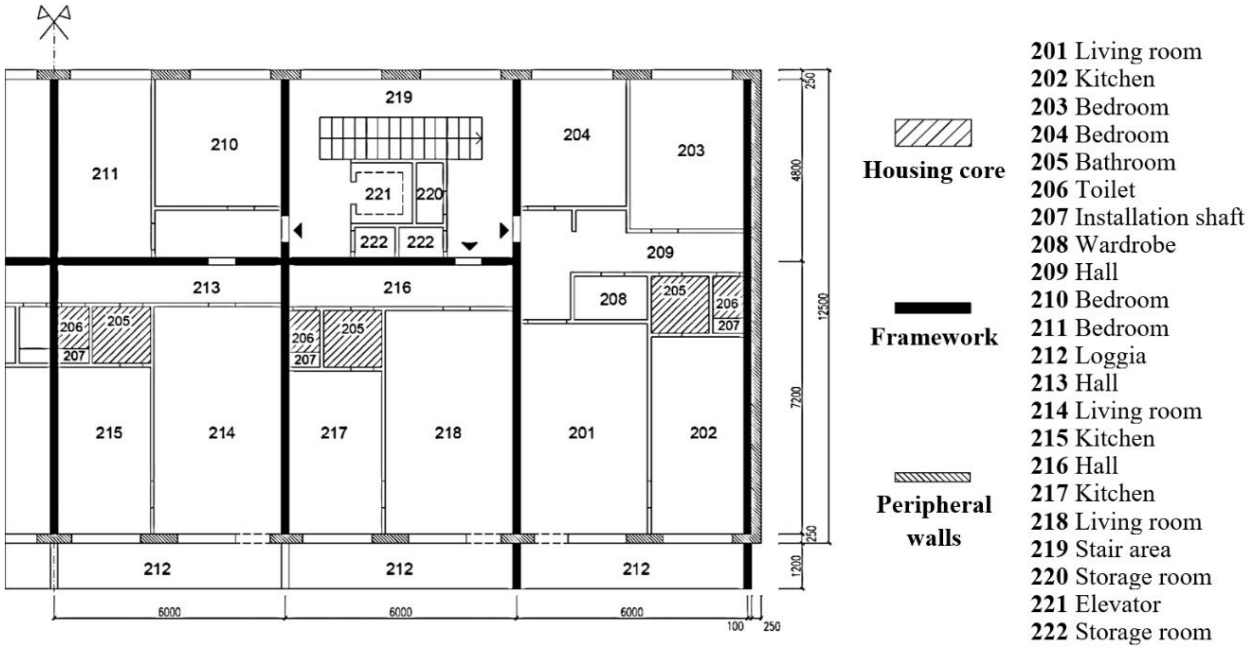

FIGURE 3: Typical floor of the panel house type T 08B KE [2]

The selected air duct is used to ventilate 3-room apartments, which are mostly inhabited by four people. The duct opens into the damping chamber, the ventilation air from the ventilation duct is removed through a vent duct cup (Table 2). Originally, the air outlet was ensured by a fan, currently the fan is not functional, or it is shut down.

TABLE 2
TERMINATION OF THE AIR DUCT

	**1**	*Vent duct cup with installed fan:* - diameter of the cup: d = 720 mm
	2	*Damping chamber:* - the space into which the ventilation duct opens, - chamber dimensions (width / length / height): W / L / H = 900 mm / 1300 mm / 400 mm
	3	*Ventilation of the air duct*

V. MEASUREMENT PREPARATION

Before installing the measuring apparatus for continuous measurement, it was necessary to obtain the overall profile of the air flow of the duct by control measurement. Nine measuring points were chosen for the square ventilation duct with dimensions of 225 x 250 mm (Fig. 4). The flow profile was obtained by control measurement. A median was created from the measured parameters.

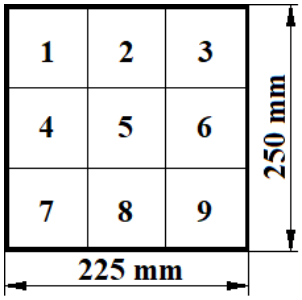

FIGURE 4: Air duct cross-section with 9 measuring points

The measuring probes (Fig. 5) were placed in point 2 to ensure the stability of the support grid with probes installed on the duct outlet. The measured results were subsequently modified by calculation coefficients, which were created by evaluating the ratio of the mean values of individual parameters to the parameter values from point 2.

FIGURE 5: Installation of measuring equipment

VI. MEASUREMENT PROCESS

The measurement took place nine days during the heating season continuously. One measurement interruption was recorded during the measurement. It was necessary to replace the batteries in data logger Almemo 2390-8. After the measurement, the measured data was downloaded to the computer for subsequent processing.

VII. DATA PROCESSING

The measured data were transferred to the spreadsheet editor MS Office EXCEL and then processed. Measured air parameters at the outlet of the ventilation duct:

7.1 Air flow rate

The flow rate of the outgoing air is shown by graphs with values processed in half-hour intervals. The air flow during the 4 working days of the week (Fig. 6a) is relatively stable. The outgoing air reached a velocity between 1.5 and 2.6 meters per second. From the course of air flow velocities, it is possible to deduce approximately when residents get up, that is, when they use the bathroom to a greater extent, etc.

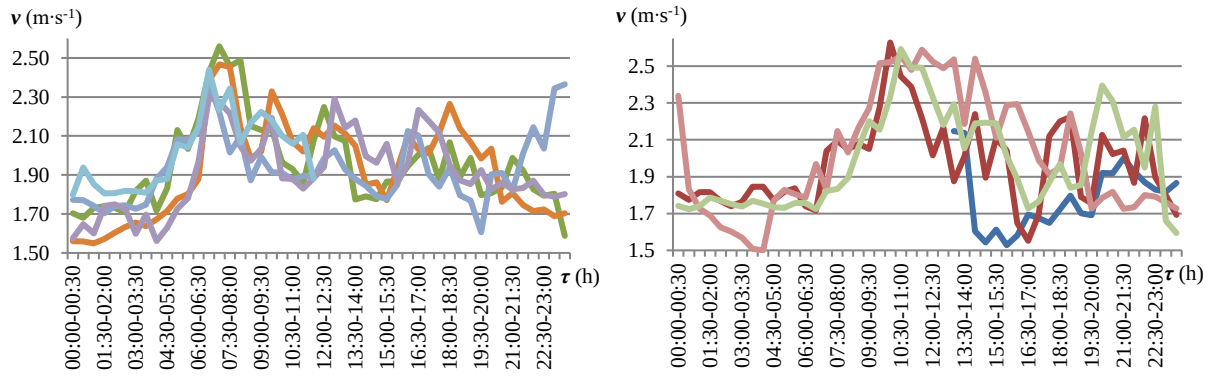

a. working days ***b. weekends***

FIGURE 6: The air flow rate in monitored period

As for the weekend ventilation air flow profile, the following graph (Fig. 6b) shows that most residents are at home and engaged in various activities (cooking, cleaning). The later time of getting up and therefore using the bathroom and toilet is also evident. The outgoing air reached a velocity between 1.5 and 2.6 meters per second during the weekends. Compared to the working days of the monitored period, the maximum flow velocity values were recorded later, approximately between 10:00 a.m. to 12:00 p.m.

7.2 Ventilation air temperature

An overview of the ventilation air temperatures at the outlet of the ventilation duct is shown in the following graphs (Fig. 7).

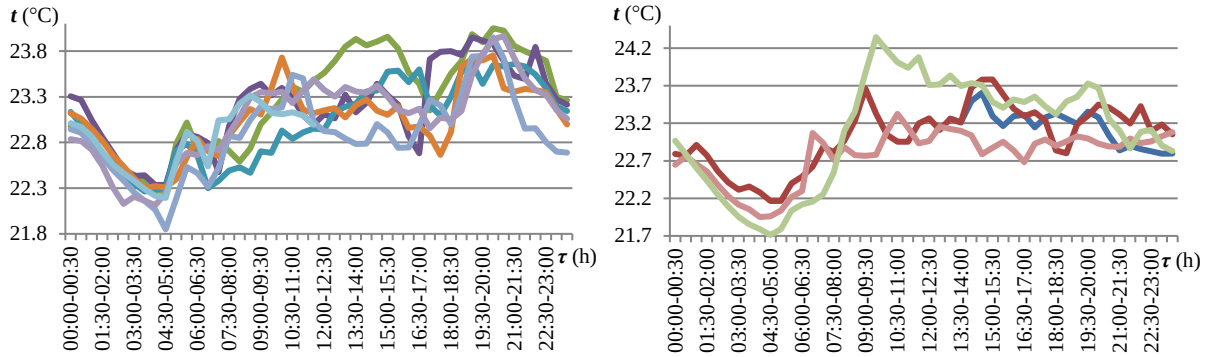

a. working days *b. weekends*

FIGURE 7: Ventilation air temperatures in monitored period

During working days, the temperature of the ventilation air reached a maximum of 24 °C, the minimum temperature was 21.8 °C. At approximately the same time, the probes recorded an increase in temperature and air flow speed.

The dependence of temperature and flow speed was also confirmed when comparing the graphs of the observed weekend period. The temperature range during the weekends was between 21.7 °C and 24.3 °C.

7.3 Relative air humidity

The humidity of the air developed depending on the temperature and the speed of the air flow in the duct. Relative air humidity reached a maximum of 50 %, its minimum was 35 %. The largest dispersion of values in the monitored period was recorded between 8:30 a.m. to 2:30 p.m.

The course of the relative humidity values in Fig. 8a indicates that after the evening hygiene of the residents, the bathrooms are gradually ventilated. A decrease in relative humidity values is recorded until approximately 3:00 p.m., which indicates the approximate time of arrival of residents from work, school, etc.

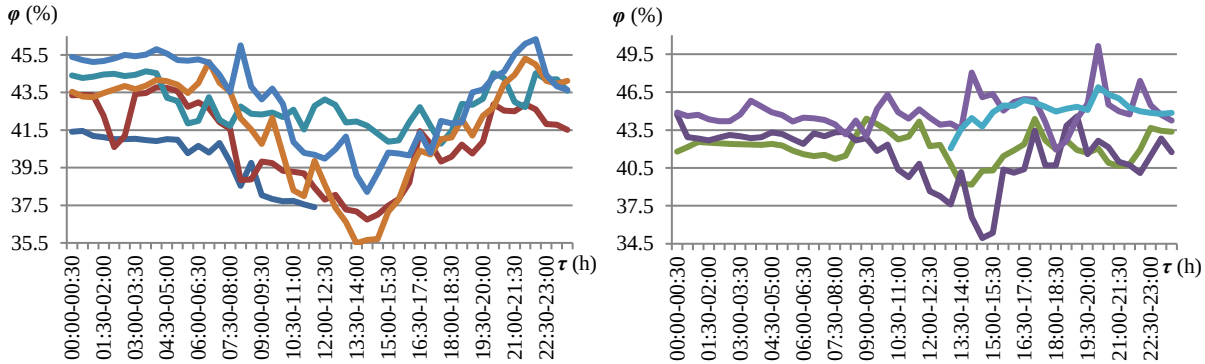

a. working days *b. weekends*

FIGURE 8: Relative air humidity

For a complete analysis of the development of relative humidity, a graph for weekend days is also presented (Figure 8b). Relative humidity values show a stable trend from midnight to approximately 10:00 a.m. with relative humidity values ranging from 41.2% to 45.8%. It can be assumed that residents get up around 10:00 a.m. on weekends.

VIII. CONCLUSION

The results of the measurements capture the basic parameters of the indoor air. Based on the results of the measurements, it is necessary to evaluate with further analyzes whether the air circulation is sufficient to ensure a healthy internal environment of the building with a subsequent proposal of solutions on how to achieve and maintain a healthy internal environment without increasing costs in connection with the need for increased ventilation. We plan to process these data for the calculation of heat losses through ventilation.

IX. ACKNOWLEDGEMENTS

This paper was written with the financial support from the VEGA granting agency within the project solutions No. 1/0626/20 and No. 1/0532/22 from the KEGA granting agency within the project solutions No. 012TUKE-4/2022 and with financial support from the granting agency APVV within the Project Solution No. APVV-15-0202, APVV-21-0274 and APVV-20-0205.

REFERENCES

[1] Table 1: Products of AHLBORN® company. Product´s website AHLBORN®. <www.ahlborn.com/en_UK/company>. (accessed 20.09.2022)

[2] Ministry of Construction and Regional Development of the Slovak Republic. Interventions in the Load-bearing Structures of Panel Houses. 2nd Edition. Bratislava, 2008. Pages 66-68. ISBN-978-80-89073-14-6.

[3] Encyclopedia of Building & Environmental Construction, Diagnosis, Maintenance & Repair. Air Flow Rate (CFM) Measurement. <https://inspectapedia.com/aircond/Air-Flow-Rate-Measurement.php>. (accessed 20.09.2022)

[4] J.D. Posner, C.R. Buchanan, D. Dunn-Rankin. Measurement and prediction of indoor air flow in a model room. In: Energy and Buildings. Volume 35, Issue 5, June 2003, Pages 515-526. ISSN: 0378-7788.
<https://www.sciencedirect.com/science/article/pii/S0378778802001639>. (accessed 20.09.2022)

[5] Indoor Air Hygiene Institute. Relative Humidity (RH) and Actual Humidity (AH) Explained.
<https://www.indoorairhygiene.org/humidity-explained/>. (accessed 20.09.2022).

Assessment of Physicochemical Parameters of Soils Contaminated with Petroleum from Eleme Port Harcourt, Nigeria

U.P. Ojukwu[1*], A.N. Eboatu[2]

[1]Department of Polymer and Textile Engineering, Nnamdi Azikiwe University Awka
[2]Department of Chemistry, Nnamdi Azikiwe University, Awka
*Corresponding Author

Received: 14 October 2022/ Revised: 25 October 2022/ Accepted: 05 November 2022/ Published: 30-11-2022

Abstract— *The study was conducted to examine the physicochemical parameters of soils contaminated with petroleum using nonpetroleum contaminated soil as control. Six petroleum contaminated soil samples from Eleme, Port Harcourt and one non petroleum contaminated soil sample from Awka were analyzed for pH, texture, moisture content, bulk density, total organic carbon, total organic nitrogen, total organic matter and total petroleum hydrocarbon. Some pH of the soil samples were acidic while others were alkaline and ranged from 5.26-7.84. The textural class of the petroleum contaminated soils (A-F) were silty clay loam while that of the non petroleum contaminated soil (G) was sandy loam implying that samples A-F are somewhat clayey and sample G almost sandy. Total moisture content of petroleum contaminated soils and their water holding capacity were higher than that of the control and fell in the ranges 0.50-40.56% and 13-29% respectively. Total organic carbon (TOC) and Total organic matter (TOM) of petroleum contaminated soils were higher than that of the non petroleum contaminated soil and were within the ranges 7.29-15.09% and 12.57-26.02% respectively. Total organic nitrogen result follow the same pattern with the non petroleum contaminated soil having the least value. The range was 0.365-0.755%. Bulk density results were within the range of 0.80-1.42g/cm^3. The uncontaminated soil (G) had less amount of organic matter in it as a result, the bulk density was the highest (Olaitan and Lombin, 1984). The total petroleum hydrocarbon (TPH) content ranged from 107.5305-626.4060 mg/kg with that of the non petroleum contaminated soil being the least. The results indicated that petroleum contamination affected the physicochemical properties of the soils analyzed. Regular soil assessment is recommended so as to avert any ugly incidence which may occur.*

I. INTRODUCTION

Contamination of the environment by petroleum products from variety of sources represents one of the most frequent contaminations {Mracnova et al.,1999). This is due to the growing demand and supply of fuel oil and new chemicals by the industrialized society of the twenty-first century (Jaffe,1991). High concentration levels of hydrocarbons present in contaminated sites can pose a health risk to humans, plants and animal lives as they are carcinogenic, mutagenic and toxic (Ribes et al., 2003, Freitag et al., 1985 and DEC,1992).

Oil contamination can also affect soil physical and chemical properties (Wang et al., 2013). Soil temperature, total organic carbon, pH, microbial community, available phosphorus and other soil chemical properties are affected (Aislabie et al., 2004, Townsend et al., 2003, Ekundayo and Obuekwe, 2000, Hu et al,. 2006), Oil causes anaerobic environment in the soil by smothering soil particles and blocking air diffusion in the soil pores. In addition, crude oil contaminated soils are hydrophobic compared with pristine sites (Quyum et al., 2002).

An assessment of the physicochemical parameters of petroleum contaminated soils from Eleme, Port Harcourt was embarked upon to monitor the levels of contaminants which can accumulate toxic proportions. The oil finds its way to soil through leakages from pipelines, underground and surface fuel storage tanks, indiscriminate spills, and careless disposal of wastes (Okop, and Ekpo, 2012). Despite improvements to the technical conditions of sites involved in the production, storage and distribution of liquid fuels, the threat to the environment posed by petroleum substance is still very real (PIEP,1995).

II. MATERIALS AND METHOD

2.1 Study Area

Eleme coordinates are 4.7994ºN, 7.1198º E. It is located at east of Port Harcourt and covers an area of 138km^2. At 2006 census, it had a population of 190,884. Precipitation in Port Harcourt averages 2708mm and the average annual temperature is 26.4ºC. The average annual relative humidity is 71.0% (https//weather and climate.com). Awka is found in the south eastern part of Nigeria. It is the capital of Anambra State and is located on Latitude 6º09′N and Longitude 7º12′E. The climate is tropical with an annual rainfall of about 11,450mm, average temperature of 28ºC and relative humidity of 91% at dawn (Nwangwu, 2015).

2.2 Sample Collection

Samples from both petroleum contaminated soils Eleme, Port Harcourt (A-F) and non petroleum contaminated soil Awka (G) were collected from a depth of 0-12 cm with soil auger (Okop and Ekpo, 2012). Five samples were randomly collected and mixed to form a representative sample (Edori and Iyama, 2017). The samples which were more than 1kg were transported to the laboratory for immediate analysis.

2.3 Sample Analysis

The pH was determined by the method of APHA (2000). The soil moisture was estimated by the method of Ibitoye (2006).

The textural class was determined by the method of Brady and Weil (2013). The methods proposed by Page (1982), Ibitoye (2006) and Head (1992) were used for the determination of organic matter, organic carbon and organic nitrogen. The total hydrocarbon content was determined by the method described by AOAC, 1990). The bulk density of the soil was determined by the method adopted by Olaitan and Lombin (1984).

III. RESULTS AND DISCUSSION

The pH of the soils samples ranged from 5.26-7.84 as presented in Table1.This is comparable with those obtained by Adoki (2012) for soil samples from borehole drilling at a legacy spill site in Eleme Port Harcourt.

TABLE 1
PHYSICOCHEMICAL PARAMETERS OF SOIL SAMPLES

	Sample A	Sample B	Sample C	Sample D	Sample E	Sample F	Sample G
pH	5.26	5.37	7.69	7.64	7.79	7.84	5.37
Texture	Silty clay loam	Silty clay loam	Silty clay loam	Silty clay loam	Silty clay loam	Silty clay loam	Sandy loam
Moisture content (%)	40.56	16.28	15.61	11.73	19.76	20.48	0.50
Bulk density (g/cm^3)	0.80	0.94	0.90	1.03	1.05	0.95	1.42
Total organic carbon (%)	14.41	15,09	10.68	12.40	10.85	10.68	7.29
Total organic nitrogen (%)	0.721	0.755	0.534	0.620	0.543	0.534	0.365
Total organic matter (%)	24.84	26.02	18.41	21.38	18.71	18.41	12.57
Total petroleum hydrocarbon (mg/kg)	620.9427	319.2833	626.4060	620.9427	163.3685	148.7637	107.5305

The pH of the environment affects the speed and direction of biological processes in the soil and is one of the factors that influence the decomposition of hydrocarbons by microorganisms in the environment (Hawrot-Paw, 2010). According to Arias (2005), soil pH plays the greatest influence on availability of nutrients to plants and the type of organism found in the soil. Although plants have begun to thrive under varying pH conditions, the optimum pH for most agricultural soils is between 5.5-7.5 QDEHP, (2017). As soil becomes increasingly acidic, important nutrients like phosphorus become less available to plants which result in reduced crop yield.

The textural classes of the petroleum contaminated soils are silty clay loam in contrast with the sandy loam of non petroleum contaminated soil (control). The percentage of sand, clay and silt are categorized as textural class. Soil texture is a measure of the physical properties of the soil such as plasticity of the soil, water retention capacity, soil productivity, soil permeability and ease or toughness of tillage of the soil (Brady, 1996). Soills with high percentage of clay have the potential to hold more water within the particles (Osuji, 2007). Sandy soils retain little water and therefore percolation of water through it is high and so promotes ground water contamination while clayey texture prevents water percolation (Schulte, 1999).

The total moisture content of the soils varied from 0.50 to 40.56% with those of the petroleum contaminated soils being higher than the non petroleum contaminated soil. The results are similar to those of Azlan et al., (2012) and are in agreement with the findings of Wang et al., (2013) which stated that hydrocarbon contamination can increase soil total organic carbon. Oil clogs the pores of soil particles and thus hinders evaporation of water (Olaitan and Lombin, 1984). Aggregation due to force of adhesion existing in oil particles is responsible for the high moisture content of petroleum contaminated soils (Atkins and Jones, 1999). Also sandy soil retains very little water while clay will hold the maximum amount. Any soil with high concentration of organic components has the capacity to retain water for a long time and the drying takes longer time than usual. High moisture content is due to de-aeration which displaced air in the soil and also oxygen content of the soil and decreased microbial activity (Brady and Weil, 2008).

The water holding capacity of soils fell in the range 13-29%. These are comparable with those of the petroleum contaminated soils which are silty clay loam in texture and have higher water holding capacity than the non petroleum contaminated soil which is sandy loam. Oil blocks air diffusion in the soil pores and affects soil microbial communities (Townsend et al., 2003). The blockage of air diffusion also reduces pore spaces which results in an increase of water holding capacity and of the humidity needed for bacterial growth which eventually increases the total organic carbon and soil organic matter content. The presence of large pores results in an decrease of water holding capacity and of the humidity needed for bacterial growth (Azlan et al., 2012). Also, the presence of a relatively high percentage of clay in samples A-F accounts for the ability of the soils to hold more water within the particles.

The bulk density of samples were within the range 0.80-1.42 g/cm^3. Clay soils have bulk density values ranging from 1.10to1.40g/cm^3. Loams, sandy loams and sand have bulk densities ranging from 1.20-1.80g/cm^3 (Olaitan and Lombin, 1984).

The total petroleum hydrocarbon content of the samples compares favourably with those of Okop and Ekpo, (2012) and Adoki, (2012). The results fell within the range 107.5305- 626.4060 mg/kg and increased in the following order C>A, D >B>E>F>G. The petroleum contaminated samples show elevated concentrations of TPHs when compared with the control (non-petroleum contaminated sample) and could be attributed to oil spilling effect at the sampled areas (Asaolu, 2000). Hydrocarbon contamination can increase soil total organic carbon (Ekundayo and Obuekwe, 2000) and change soil pH values (Hu et al., 2006). The total organic carbon (TOC) content varied from 7.29 to 15.09% and the total organic matter (TOM) content varied from 12.57 to 26.02%. The total organic nitrogen (TON) range is 0.365-0.755%. The results of the TOC and TOM agree favourably with those Edori and Iyama (2017). The TOC, TOM and TON of petroleum contaminated soils are higher than that of the control and this is in agreement with the work of Nwankwoala and Ememu (2018). Soil organic matter (SOM) is the soil nutrient pool and the changes will affect the quality and quantity of soil fertility. SOM stabilizes soil pH which plays an important role in controlling the supply of nutrients and their availability for plant intake (Azlan et al., 2012). Concentration and turnover of SOM is affected by the formation of a large number of factors such as climate (Ganuza and Almendros, 2003), topography (Burke, 1999), vegetation (Finzi et al., 1998), the parent material (Spain, 1990) and management (Yang and Wander, 1999). The soil organic carbon is obtained by decomposition of the plants, animals and anthropogenic sources such as chemical contaminants, fertilizers or organic rich waste (Kong et al., 2009).

Higher levels of organic nitrogen are observed in samples A-F (petroleum contaminated soils) than in sample G (control). This again is due to increased level of decayed organic matter and contamination by petroleum in samples A-F. Nitrogen compounds detected in petroleum include polycyclic aromatic amines, carbazole, benzocarbazole, heterocyclic aromatics, triaromatic azaarenes, nitrogen heterocycles as well as diaromatic nitrogen bases (Thomas and Ringen, 1985).

REFERENCES

[1] Mracnova, R, Sojak, L, kubinec, R and Kraus, A (1999). Analysis of Petroleum Hydrocarbons in Soil from View of Bioremediation Process Comenius University Bratislava (Research Grant No., UK/ 3673/99) and Grant Agency VEGA (Grant No 1/6108/99, Slovakia, p436.

[2] Jaffe,R. (1991.Fate of Hydrophobic Organic Pollutants in the Aquatic Environment, A Review, Environ.Pollut. 69:237-257.

[3] Ribes,A, Grimalt, J.O., Torres, C.J and Cuevas, E.(2003). Polycyclic Aromatic Hydrocarbons in Mountain Soils of the Subtropical Atlantic, Journal of Environ. Qual., 32:977-987.

[4] Freitag, D, Ballhorn, L., Geyer,H., and Korte, F., (1985). Environmental Hazard Profile of Organic Chemicals, Chemosphere, 14:1589-1616.

[5] Department of Environmental Conservation-DEC (1992). Petroleum Contaminated Soil Guidance Policy, Spills Technology and Related Series (STARS), Revised, New York State.

[6] Wang, Y., Feng, J., Lin, Q., Lyu, X, Wang, X. and Wang, G. (2013). Effects of Crude Oil Contamination on Soil Physical and Chemical Properties in Momoge Wetland of China, Chin. Geogra. Sci. 23(6):708-715.

[7] Aislabie, J.M., Balks,M.R., Foght, J.M. et al., (2004). Hydrocarbon Spills on Antarctic Soils: Effects and Management, Environmental Science and Technology, 38(5):1265-1274.

[8] Townsend, G.T., Prince, R.C and Suflita, J.M. (2003). Anaerobic Oxidation of Crude Oil Hydrocarbons by the Resident Microorganisms of a Contaminated Anoxic Aquifer, Environmental Science and Technology, 37 (22):5213-5218.

[9] Ekundayo, E., Obuekwe, O. (2000). Effects of an Oil Spill on Soil Physicochemical Properties of a Spill Site in a Typic Udipsamment of the Niger Delta Basin of Nigeria, Environmental Monitoring and Assessment, 60(2):235-249.

[10] Hu, Y., Wang, S and Yan, S. (2006). Research Advances on the Factors Influencing the Activity and Community Structure of Soil Microoganism, Chinese Journal of Soil Science, 37 (1):170-176.

[11] Quyum, A., Achari, G., Goodman, R. (2002). Effect of Wetting and Drying and Dilution on Moisture Migration through Oil Contaminated Hydrophobic Soils, Science of The Total Environment, 296 (1):77-87.

[12] Okop, I.J. and Ekpo, S.C. (2012). Determination of Total Hydrocarbon Content in Soil after Petroleum Spillage, Proceedings of the World Congress on Engineering, vol. 111, July 4-6, London, Uk.

[13] Polish Institute of Environmental Protection –PIEP, (1995). Methodological Guidelines Concerning the Degree of Contamination of Soil and Groundwater with Petroleum Products and Other Chemical Substances in Remediation Processes, Warazawa.

[14] Edori, O.S. and Iyama, W.A. (2017). Assessment of Physicochemical Parameters of Soils from Selected Abbatoirs in PortHarcourt, Rivers State, Nigeria, J.Environ. Anal, Chem. 4:194.

[15] APHA, (2000). Standard Methods of Examination of Water and Wastewater, American Public Health Association, Washington DC.

[16] Olaitan, S.O. and Lombin, G. (1984). Introduction to Tropical Soil Science, Macmillan Education Ltd, London, pp1-43.

[17] Brady,N.C. and Weil, R.R.(2013). The Nature and Properties of Soils, Pearson Education Inc., India, p130.

[18] Page, A.L. (1982). Methods of Soil Analysis Part 2, Chemical and Microbiological Properties, 2nd edition, Madison Wisconsin, U.S.A., pp202, 561-570.

[19] Ibitoye, A.A. (2006). Laboratory Manual on Basic Soil Analysis, 2ndedn., Foladave Nig Ltd, Akure, Ondo State, Nigeria, pp6-35, 76.

[20] Head, K.H. (1992). Manual of Soil Laboratory Testing (Soil Classification and Compaction Tests) 3rd edition, Whittles Publishing, Scotland, UK, 1:282-283.

[21] Association of Official Analytical Chemists (1990). Official Methods of Analysis, 15th edition, Washington DC, USA,

[22] Adoki, A. (2012). Soil and Groundwater Characteristics of a Legacy Spill Site, J. Appl. Sci. Environ. Manage,16(1):113-123.

[23] Hawrot-Paw, M. (2010). Biodegradation of Selected Petroleum Products in Variable Temperature Conditions and pH of the Environment, Acta Sci. Pol., Formatio Circumiectus 9(4):17.

[24] Arias, M.E., Gonzalez-Perez, J. A., Gonzalez-Villa, F.J., Ball, A.S.(2005). Soil Health: A New Challenge for Microbiologist and Chemists, Int. Microbiol 8:13-21.

[25] Queensland Department of Environment and Heritage Protection-QDEHP (2017).

[26] Brady, N.C. (1996). The Nature and Properties of Soils (eds. 11th), Macmillan, New York, pp621.

[27] Osuji, L .C. and Nwoye, I.(2007). An Appraisal of the Impact of Petroleum Hydrocarbons on Soil Fertility: The owaza Experience, Afrj. Agri Res 2:318-324.

[28] Schulte, E.E. (1999). Soil and Applied Chlorine, College of Agriculture and Life Sciences, University of Wisconsin-Madison and University of Wisconsin Extension, Cooperative Extension, Wisconsin, USA.

[29] Azlan, A., Aweng, E.R., Ibrahim, C.O., NoorHaidah, A. (2012). Correlation between Soil Organic Matter, Total Organic Matter and Water Content with Climate and Depths of Soil at Different Land Use in Kelantan, Malaysia, J.Appl. Sci. Environ. Manage., 16(4)353-358.

[30] Atkins,P and Jones, L, (1999).Chemical Principles , W.H. Freeman and Company New York, p201.

[31] Brady, N.C and Weil,R.R. (2008).Soil Colloids : Seat of Soil Chemical and Physical Acidity, The Nature and P roperties of Soils, Pearson Education Inc., Upper Saddle River, NJ, USA, pp311-358.

[32] Asaolu, S.S. (2000). Total Hydrocarbon Content in water and Sediment Samples from Ondo State Coastal Area, The Journal of Technoscience, 4:20.

[33] Edori, O.S and Iyama, W.A. (2017). Assessment of Physicochemical Parameters of Soils from Selected Abattoirs in Port Harcourt, Rivers State, Nigeria J.Environ. Anal. Chem. 4:194.

[34] Ganuza, A.G and Almendros, (2003). Organic Carbon Storage in Soils of the Basque Country (Spain): The Effect of Climate, Vegetation Type and Edaphic Variables, Biology and Fertility of Soils, 37: 154-162

[35] Burke, I.C.(1999). Spatial Variability of Soil Properties in the Short Grass Steppe: The Relative Importance of Topography, Grazing, Microsite and Plant Species in Controlling Spatial Patterns, Ecosystems, 2: 422-438

[36] Finzi, A .C. Breemen, N.V.and Canham, C.D.(1998).Canopy Tree Soil Interactions Within Temperate Forests:Tree Species Effects on Carbon and Nitrogen, Ecological Applications,8:440-446.

[37] Spain, A.V. (1990). Influence of Environmental Conditions and Some Soil Chemical Properties on the Carbon and Nitrogen Contents of Soil Tropical Australian Rainforest Soils, Australian Journal of Soil Research, 28:825-839

[38] Yang, X.M and Wander, M.M. (1999). Tillage Effects on Soil Organic Carbon Distribution and Storage in a Silt Loam Soil in Illinois, Soil and Tillage Research,52:1-9

[39] Kong, X.B, Dao,T.H., Qin, J, Qin, H, Zhang, F. et al.,(2009). Effects of Soil Texture and Land Use Interactions on Organic Carbon in Soils in North China Cities' Urban Fringe, Geoderma, 154:86-92.

[40] Thomas, J and Ringen, S. (1985). Non Metal Elements and Compounds, Analytical Chemistry 15(5): 210R-212R.

[41] Nwangwu, C.E. (2015). Effect of Rainfall Variation on Cassava Yield in Awka, Anambra State, Unpublished Thesis, Nnamdi Azikiwe University, Awka

https//weather-and-climate.com/-month

Thermal Recovery of Lemna Minor during the Process of Obtaining Hydrogen

Lukáš Tóth[1], Romana Dobáková[2], Ivan Mihálik[3], Ľubomíra Kmeťová[4]

Department of Power Engineering, Faculty of Mechanical Engineering, Technical University of Košice, Slovakia
*Corresponding Author

Received: 01 November 2022/ Revised: 09 November 2022/ Accepted: 16 November 2022/ Published: 30-11-2022

Abstract— *The aim of the article is a theoretical evaluation of the possibilities of using fast-growing aquatic plants, specifically Lemna minor, for the mass production of biomass suitable for the subsequent thermal treatment during the blue hydrogen production process. Much laboratory research has demonstrated the possibility of increasing the volume of biomass under controlled conditions, using water from wastewater treatment plants, or water contaminated with organic residues (faeces) from organic production. Hydroponic cultivation in controlled conditions has shown the possibilities of removing hazardous substances from wastewater, possibly reducing their contamination and at the same time, producing organic biomass with more favourable properties than in the case of dendromass.*

Keywords— Lemna minor, biomass, hydrogen, thermal treatment.

I. INTRODUCTION

The increasing effort of producing hydrogen, which is not tied to fossil sources, is the incentive to search for other methods of its mass production. In addition to methods that use water electrolysis for obtaining hydrogen, there is also a gradual expansion of methods that use organic substances to produce hydrogen, which subsequently undergo thermal recovery. In addition to synthesis gas, products of such thermal recovery are also various oils, tars and solid residue, which can subsequently be used in various industrial areas. The use of fast-growing biomass also enables the storage of solar energy by a method other than just in the form of batteries. Biomass stores solar energy transformed into lipids and other organic energy stores, while it´s considered a carbon-neutral source, since during its growth, an equivalent amount of CO2 is absorbed from atmosphere to the amount of CO2 released during its combustion process. Of particular importance is the potential of biomass-derived fuels to replace petroleum-based fuels, such as gasoline, jet fuel and diesel fuel, and thereby decreasing the dependence on imported oil. Hydrocarbon-based fuels offer several advantages over oxygenated biofuels (e.g. biodiesel, bioethanol), in that they have a higher volumetric energy content and are compatible with already existing infrastructure for the import and distribution of fuel [1].

II. LEMNA MINOR

Lemna minor is one of the smallest and fastest-growing flowering plants on earth. It´s an extremely reduced floating freshwater plant, with one, two, three or four leaves, each of which has one root hanging in water. The root is 1-2 cm long. Leaves are oval, 1-8 mm long and 0,6-5 mm wide, light green colour, with three (rarely five) veins and small air spaces that allow the plant to float on the water surface. 1 As an aquatic plant, Lemna minor is commonly used to remove excess nutrients (e.g. nitrogen and phosphorus) and toxic metals from agricultural and municipal wastewater. For more than 30 years, researchers

have been demonstrating the potential use of sewage grown Lemna minor as a possible food supplement for livestock. Due to considerable growth rate and high protein content, protein productivity can be ten times higher than that of soybeans, without encroaching on arable soil necessary for food growing [2].

The growth rate of Lemna minor in the wastewater is given in an open uncontrolled environment at the level of 29 $g \cdot m^{-2} \cdot day^{-1}$, which equals 104 $t \cdot ha^{-1} \cdot year^{-1}$. The rate of removal of excessive amount of nitrogen and phosphorus in wastewater was at the maximum of 3,36 $g \cdot m^{-2} \cdot day^{-1}$ for nitrogen and 0,59 $g \cdot m^{-2} \cdot day^{-1}$ for phosphorus [3]. By subsequent thermal processing it´s possible to regain phosphorus originally obtained from wastewater and use it for further technological purposes.

In addition to nutritional values, which are the main indicator for the use of biomass produced from Lemna minor for livestock fattening, the biomass also contains significant amounts of starch, which, unlike cellulose, can be easily converted into bioethanol that can serve as a potential source of biofuel produced in wastewater. Overall decrease in the contamination of wastewater from organic production with the most important components can be observed in Table 1.

TABLE 1
COMPOSITIONS OF SWINE LAGOON WASTEWATER AND SH MEDIUM BEFORE AND AFTER CULTURE OF LEMNA MINOR. [4].

Elements	$NO_3^- - N$ $(mg \cdot l^{-1})$	$PO_4^{3-} - P$ $(mg \cdot l^{-1})$	$CO(NH_2)_2$ $(mg \cdot l^{-1})$	$NH_4^+ - N$ $(mg \cdot l^{-1})$	$total\ sugars$ $(mg \cdot l^{-1})$	pH
SL wastewater						
Day 0	0.8 ± 0.1	16.3 ± 0.6	16 ± 0.1	56.1 ± 0.9	36.3 ±0.2	7.4
Day 18	0.2 ± 0.2	4.1 ± 0.3	0.2 ± 0.1	0	1.6 ± 0.1	6.8
Removal (%)	75.0	74.8	87.5	100	95.6	-
SH medium						
Day 0	495.3	85.1	0	35.5	10 000	5.6
Day 27	24.2 ± 2.1	10.4 ± 1.2	0	0	250.6 ± 22.3	6.5
Removal (%)	95.1	87.8	0	100	97.5	-

As can be seen in Tab.1., according to the research by Jianfeng Xu et al., there´s a significant decrease in wastewater contaminants from agricultural production. A decrease in contamination in the case of wastewater in municipal wastewater treatment plants can be assumed at the same level.

III. INCREASING THE YIELD OF LEMNA MINOR PER 1 M2 OF USEFUL AREA

Increasing the yield of biomass produced by Lemna minor is conditioned by maintaining an appropriate water surface population density. With the increasing population density of living biomass on the water surface, there is a significant slowdown in the production of new offshoots and thereby a slowdown in the biomass production. The growth rate is also significantly related to the ambient temperature and with rising temperature, the reproduction rate increases approximately linearly until the optimal population density is reached.

As stated by E. H. van Nes et al., the highest growth rate 0,30 d^{-1} was observed at biomass population density of 10 $gDW \cdot m^{-2}$. During their experiments, in the measurement of growth rate they also reached a value of 26 $g \cdot m^{-2} \cdot day^{-1}$ [5], which does not significantly differ from the findings of team led by J. Cheng, although the difference could be caused by the different location

during the experiment, when the J. Cheng´s team worked in Brazil during summer, while the team led by E. H. van Nes worked in the Netherlands during the spring.

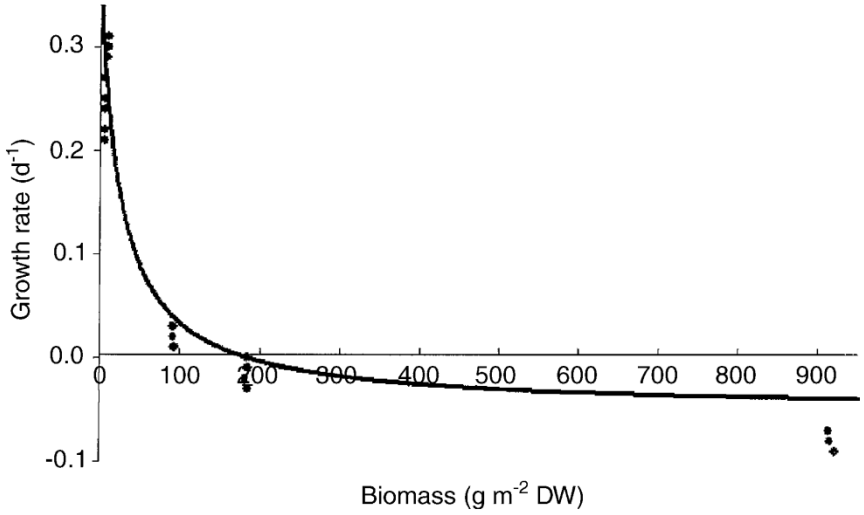

FIGURE 1: Growth rate as a function of the initial biomass of Lamna minor (gDW m^{-2}). Dots indicate the measured growth rate. The solid line represents the curve described by the model at a constant temperature of 23 °C [5].

The limitation of Lemna minor´s population density can by circumvented by the industrial method of hydroponic cultivation when it is possible to place tanks with wastewater on top of each other and ensure sufficient light with the use of electric lighting.

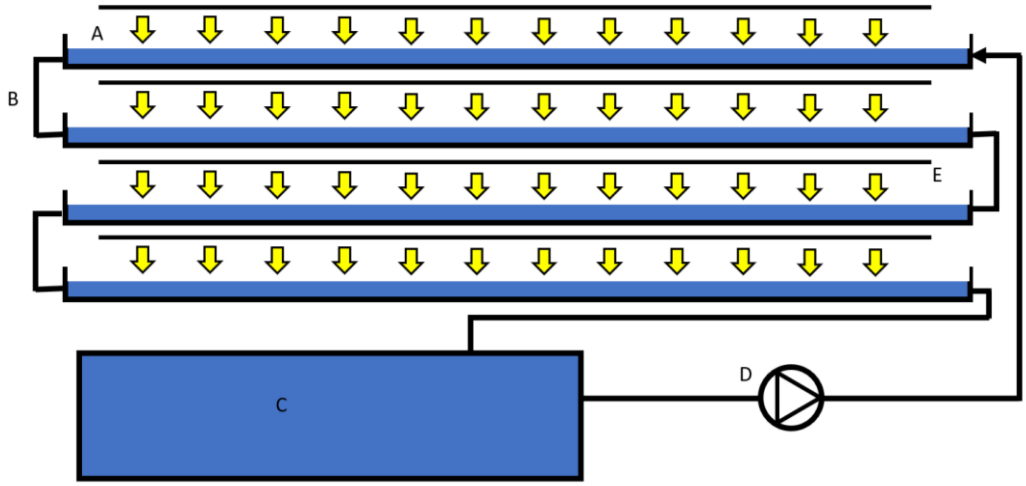

A – water reservoirs for biomass cultivation, B – connecting pipe, C – water tank with the water quality sensors, systems for adding and adjusting nutrients and systems for temperature controll, D – circulator pump, E – full-spectrum light

FIGURE 2: Simplified scheme of Lemna minor multi-layer cultivation

It is possible to implement the flow method of wastewater passage for the multilevel arrangement of tanks, when the wastewater enters the highest tank and subsequently, by the action of gravitational force, gradually passes through the lower tanks until it reaches the lowest tank, from where it flows farther for further cleaning, or closed circulation, when the large-volume container is filled with contaminated water, which then passes through the tank system using a circulator pump and a gravity, until the desired decrease in contamination, primarily by phosphorus and nitrates, is reached.

In hydroponic cultivation, it is possible to use technical spaces that have no practical use, because they are located underground without windows, have poor ventilation or other unfavourable properties, or buildings directly built for the purposes of hydroponic cultivation. During the theoretical analysis, it is possible to work with a closed room with dimensions 10x5x2,5

meters, where it would be possible to place wastewater tanks with a spacing of 25 cm. The given arrangement would allow the increase of useful area from 50 m^2 to 400 m^2. With the daily production of 29 $g \cdot m^{-2} \cdot day^{-1}$, which could be increased by lighting 24 $h \cdot day^{-1}$, a daily production of 11,6 kg DW·day-1 could be possible. If operated 360 days a year, the annual production of such a room would be cc 4175 kg DW·year [1].

IV. THERMAL TREATMENT OF DRY LEMNA MINOR

According to N. Muradov et al., the chemical analysis of dry Lemna minor is as follows (hm. %):

- humidity – 3,7.
- total volatile substances (120–950 °C) – 78,0 (including volatile substances released at 120–650 °C – 67).
- solid carbon – 8,8.
- ash – 9.5.

The final analysis of the dry sample of Lemna minor gave the following chemical composition of individual elements (%): C – 39,11; H – 6,13; O – 37,74; N – 5,52; S – 0,67

The high proportion of carbon and oxygen in the dry sample of Lemna minor indicates the formation of a significant amount of carbon dioxide and carbon monoxide, during the biomass heat treatment process. As shown by the results of N. Muradov et al., increasing the temperature of the process has a significant effect on the production of carbon monoxide in favor of the formation of carbon monoxide and hydrogen.

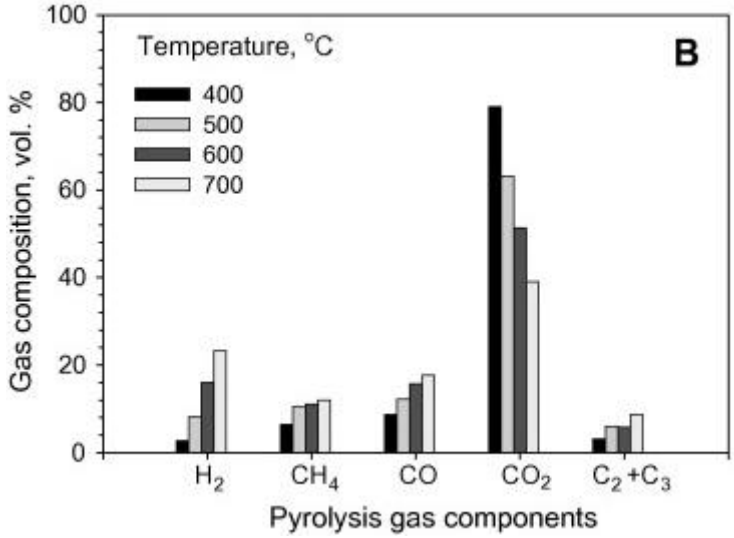

FIGURE 3: Composition of pyrolysis gas produced by Lemna minor pyrolysis depending on the pyrolysis temperature at Air flow rate of 60 $ml \cdot min^{-1}$ [6]

The amount of carbon dioxide produced as result of thermal conversion of Lemna minor to synthesis gas is too high for subsequent processing in obtaining hydrogen. By increasing the temperature of the Lemna minor thermal recovery process, or by using a plasma reactor system, an increase in the proportion of hydrogen and gases such as methane and carbon monoxide could occur, which can then be technologically processed using WGS reactors using a suitable catalyst and water vapor into carbon dioxide and hydrogen.

V. CONCLUSION

As a result of the evaluation of the many projects in the field of cultivation, use and processing of Lemna minor, it is possible to come to conclusion that the production of biomass from the mentioned plant with the use of wastewater, represents one of the ways to reduce our society's dependence on fossil fuels and dendromass, which currently represents a short-term but slow renewable compensation. The suitability of direct thermal treatment of Lemna minor to synthesis gas suitable for hydrogen production is debatable. A more suitable procedure is to use methanogenic organisms to produce methane from Lemna minor biomass, which can then be technologically modified using WGS reactors for hydrogen and carbon dioxide.

ACKNOWLEDGEMENTS

This paper was written with the financial support from the VEGA granting agency within the project solutions No. 1/0626/20 and No. 1/0532/22 from the KEGA granting agency within the project solutions No. 012TUKE-4/2022 and with financial support from the granting agency APVV within the Project Solution No. APVV-15-0202, APVV-21-0274 and APVV-20-0205.

REFERENCES

[1] Mohedano, R. A., Costa, R.H.R., Tavares, F.A., Filho, P.B.: High nutrient removal rate from swine wastes and protein biomass production by full-scale duckweed ponds. Bioresource Technology, 112 (2012), p. 98 – 104.

[2] Landesman, L., Parker, N.C., Fedler, C.B., Konikoff, M.: Modeling duckweed growth in wastewater treatment systems. Livestock Research for Rural Development, 17 (6) (2005).

[3] Bergmann, B.A., Cheng, J., Classen, J., Stomp, A.M.: In vitro selection of duckweed geographical isolates for potential use in swine lagoon effluent renovation. Bioresource Technology, 73 (2000), p. 13 – 20.

[4] Ge, X., Zhang, N., Phillips, G.C., Xu, J.: Growing Lemna minor in agricultural wastewater and converting the duckweed biomass to ethanol. Bioresource Technology, 124 (2012), p. 485-488.

[5] Driever, S.M., van Nes, E.H., Roijackers R.M.M.: Growth limitation of lemna minor due to high plant density. Aquatic Botany, 81 (2005). p. 245 – 251.

[6] Muradov, N.,Fidalgo, B., Gujar, A.C., T-Raissi, A.: Pyrolysis of fast-growing aquatic biomass – Lemna minor (duckweed): Characterization of pyrolysis products. Bioresource Technology, 101 (2010). p. 8424 – 8428.

Design of Passive Internal Heat Transfer Intensifier for Metalhydride Vessels for Mobile Applications

Filip Duda[1*], Natália Jasminská[2], Ľubomíra Kmeťová[3], Šimon Hudák[4]

Department of Power Engineering, Faculty of Mechanical Engineering, Technical University of Košice, Slovakia
*Corresponding Author

Received: 01 November 2022/ Revised: 10 November 2022/ Accepted: 20 November 2022/ Published: 30-11-2022

Abstract— *For the development of modern transport systems that meet the demanding goals of reducing greenhouse gas emissions, set in the Paris Agreement from the end of 2015, it is necessary to consider new technologies and new vehicle concepts. In addition to the contractually agreed and accelerating need to contribute to significant emissions reductions, such developments would help to replace fossil fuel energy that most countries around the world are heavily dependent from. Thus, fossil fuels cannot be part of a suitable transport system.*

The aim of this work is to design an effective passive cooling system for metal hydride pressure vessel which is used for mobile applications.

Keywords— Passive Intensifier, Metal Hydride, Hydrogen.

I. INTRODUCTION

A promising technological concept that meets the above requirements is the use of hydrogen in combination with fuel cells and an electric engine. Compared to battery electric vehicles, such an approach has the advantage that hydrogen cars could be driven for much longer distances without refuelling. But such a hydrogen-based mobility concept will be successfully implemented in the existing mass market only if hydrogen can be stored safely, quickly and in a technically advanced, economically efficient, and ecological way.

The biggest advantage of using hydrogen in mobile applications is the zero production of emissions (NO_x, CO_2) when it is burned in fuel cells. An important aspect of the applicability of hydrogen in mobile applications is its energy content. A kilogram of hydrogen has three times higher energy content compared to commonly used fuels such as gasoline (H2: 39.4 kWh·kg-1, gasoline: 12.9 kWh·kg^{-1}, CNG: 15 kWh·kg^{-1} and LPG: 14 kWh·kg^{-1}). In a volume comparison, the energy content of hydrogen is significantly lower than that of commonly used fuels (H2: 1.6 kWh·l^{-1}, gasoline: 9.5 kWh·l^{-1}, CNG: 2.5 kWh·l^{-1} and LPG: 7.3 kWh·l^{-1}). Therefore, for the efficient use of hydrogen, it is important to increase its density by compression. Currently, several methods of hydrogen storage are applied in practice:

- **Compressing hydrogen gas:** it is carried out at room temperature and the maximum pressure depends on the materials from which the vessels are made. In available cars, the hydrogen pressure is at the level of 70 MPa, and for buses, the maximum pressure is reduced to 35 MPa.
- **Hydrogen liquefaction:** a very energy-intensive process with consumption of up to 15.2 kWh per kilogram of hydrogen. Liquefied hydrogen is subsequently kept in a liquid state at a temperature of -252 °C.

- **Storage of hydrogen by adsorption on the surface of solid substances**: this is a reversible way of storing hydrogen using the attractive Van der Waals interactions of atoms of a solid substance with gas molecules, which keep them on its surface. Materials that have the largest surface area are used for this storage. They are mainly porous materials such as zeolites and activated carbon. The biggest disadvantage is the need to maintain the vessel at a liquid nitrogen temperature of up to -195 °C and at a pressure of 2.5 MPa.
- **Storage of hydrogen by absorption into metal hydrides MH**: this type of hydrogen storage is the most suitable in terms of safety. This reversible process of absorption and desorption of hydrogen can be done at room temperatures and at low pressures 0.01 - 1 MPa. Biggest disadvantage is that heat is released during absorption process, and it is necessary to heat up the metal hydride while desorption process. It is compulsory to design an effective thermal management for effective utilisation of this type of storage.

As part of the work solution, the Hydralloy® alloy was chosen, the composition of which is based on MnTiVFeZr (Fig. 1). The composition of this alloy in wt.% is shown in TAB. 1.

FIGURE 1: Applied metal hydride alloy Hydralloy®

TABLE 1
COMPOSITION OF APPLIED METAL HYDRIDE ALLOY HYDRALLOY® IN VESSELS

Element	wt.%
Mn	51,50
Ti	27,20
V	14,15
Fe	3,04
Zr	2,87
Ti+Zr	30,07
V+Fe	17,19

For the design, an alloy in the form of a powder (FIG. 1) is considered, whose grain size ranges from 0-2 mm. In FIG. 2 shows the PCI curve of three repeated measurements of the applied MH alloy at room temperature.

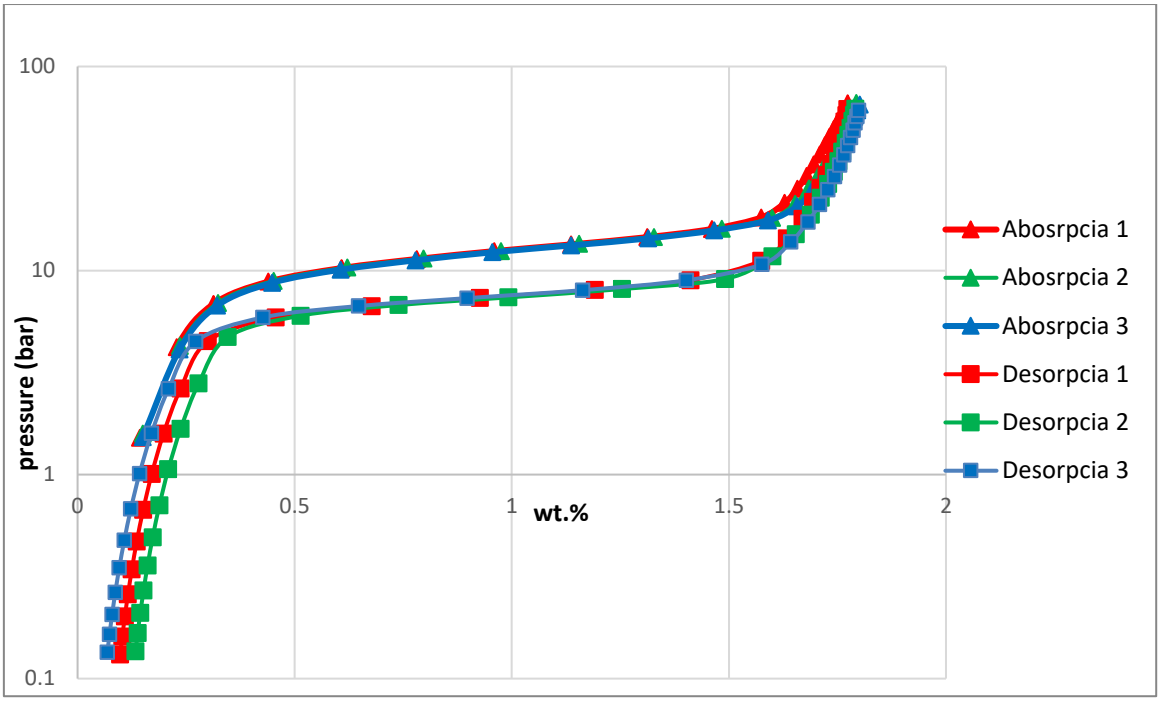

FIGURE 2: PCI curve of absorption and desorption of Hydralloy® alloy at room temperature of 3 different measurements

It can be seen from the PCI curves that the capacity of stored hydrogen at a temperature of 20 °C and a pressure of $65 \cdot 10^5$ Pa is expressed by the ratio of the weight of the absorbed hydrogen to the weight of the alloy at the level of 1.8%. Hydrogen absorption into the MH alloy structure occurs at a pressure of $11.95 \cdot 10^5$ Pa. Desorption of hydrogen from the structure of the MH alloy occurs at a pressure of $7.33 \cdot 10^5$ Pa.

Since heat is released during the absorption of hydrogen into the intermetallic structure of the metal alloy, it is necessary to remove the generated heat. The amount of released heat depends on the type of alloy used, for example, with MH alloy based on LaCeNi, 1 MJ of heat is released when 1 m^3 of molecular hydrogen is absorbed. This heat can be used in a vehicle or other mobile heating device. During the desorption of hydrogen from the structure of the MH alloy, it is necessary to bring the same amount of heat. Based on the above facts, in addition to the design of MH storage tanks, it is necessary to consider the design of temperature management, which allows heat to be removed as well as supplied.

If the MH vessel does not have temperature management and does not contain the possibility of removing the generated heat from the core of the vessel, the temperature of the MH alloy increases. As the temperature increases, the equilibrium pressure increases and the kinetics of absorption decreases. When hydrogen is desorbed from the MH reservoir without the use of forced heat supply, the temperature of the alloy drops below the ambient temperature, which is caused by absorbing heat at the expense of the internal energy of the alloy, since the heat obtained through the shell from the surroundings is insufficient, especially with larger hydrogen withdrawals.

As the temperature of the alloy decreases, the equilibrium pressure in the reservoir also decreases, and if its value falls below the minimum pressure necessary for subsequent use, the entire system may become inoperable. For these reasons, research and subsequent implementation of an internal heat exchanger or heat transfer intensifier to MH storage tanks is essential. At the same time, the heat transfer intensifiers participate in equalizing the temperature field in the volume of the powder alloy, which has a large reaction surface formed by the outer surface of the metal alloy grains.

II. DESIGN OF INTERNAL HEAT TRANSFER INTENSIFIER

Since in the process of absorption storage of hydrogen in a metal hydride vessel, due to the dissociation of the hydrogen molecule and the diffusion of H_2 atoms into the interstitial space of the crystal lattice of the metal, thermal energy is generated, it is necessary to ensure the cooling of the reservoir to eliminate pressure and temperature fluctuations. On the other hand, during the desorption of hydrogen from the metal alloy, it is necessary to heat the vessel to maintain the kinetics of the process.

The metal hydride reservoir is cooled by a passive and active element. The active cooling element is the cooling liquid that is in the space between the primary vessel and the case. A passive cooling element is a heat transfer intensifier located inside the primary reservoir that serves to dissipate the heat generated during hydrogen absorption into the metal alloy structure. By optimizing the shape of the geometry of the intensifier, it is possible to intensify the removal of heat from the reservoir core, which would improve the process of hydrogen absorption.

The geometry of the designed intensifier consists of five main and ten secondary ribs. The secondary ribs are connected to each other by primary ribs of a circular cross-section, which describes the inside diameter of the primary vessel shown in FIG. 3. The gap between the primary vessel and the intensifier is 1.

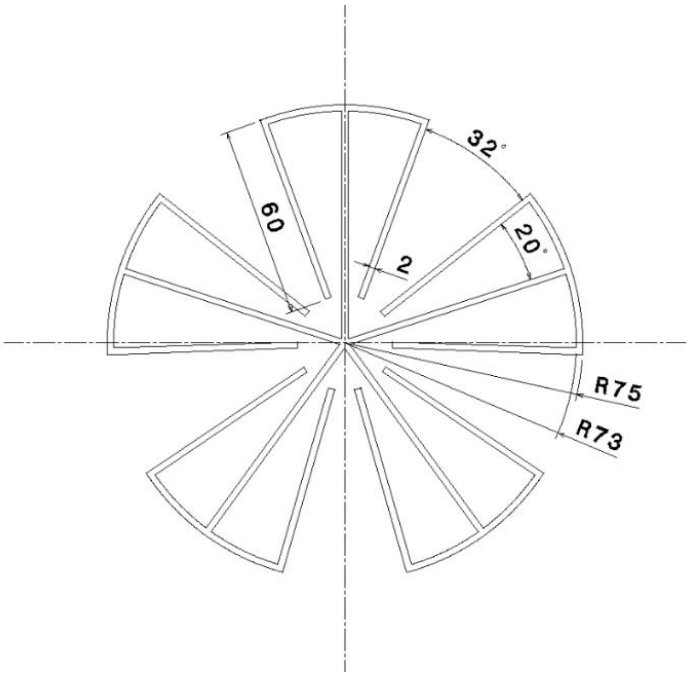

FIGURE 3: Design of internal heat transfer intensifier

In the design of the heat transfer intensifier, aluminium was used due to its good thermal conductivity of 237 $W \cdot m^{-1} \cdot K^{-1}$.

III. SIMULATION RESULTS

The temperature field in the cross-section of the vessel under investigation is shown in FIG. 4. The maximum temperature in the vessel after 1200 s which represents the time of refuelling was 89.53 °C. The hottest spots in the metal hydride were in the region between the secondary ribs. Thus, the heat is effectively removed from the core of the vessel towards the inner shell. In FIG. 5 shows the courses of maximum and minimum temperatures in the studied storage vessel after 1200 seconds of filling. On the curve of the maximum temperature, it is possible to observe the rising tendency of the temperature during almost the entire simulation, the temperature is stable in the last 200 s. The minimum temperature curve does not change from almost halfway through the simulation and remains at the same value of 30.13 °C until the end of the simulation. In FIG. 5 also shows the difference between maximum and minimum temperatures in ΔT.

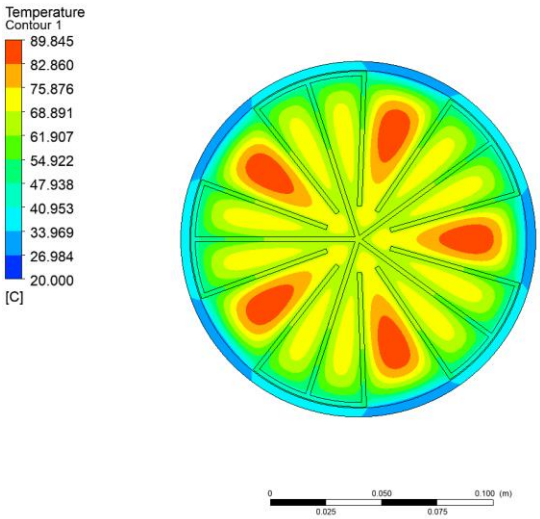

FIGURE 4: Generated temperature field after 1200 seconds of vessel filling.

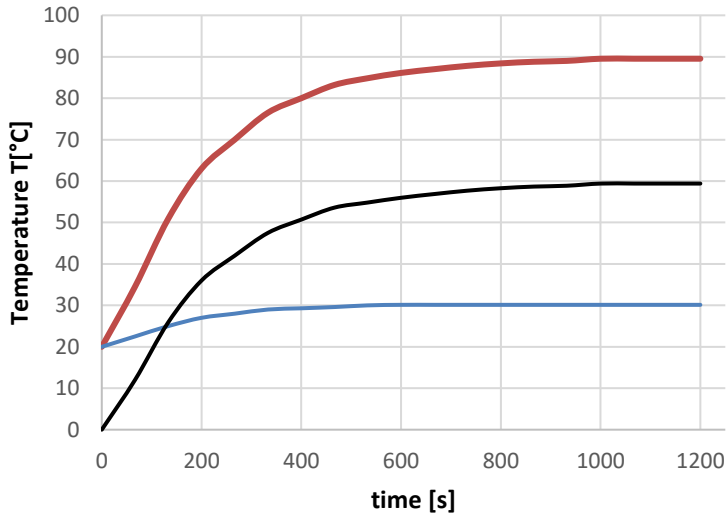

FIGURE 5: Course of minimum (blue) and maximum (orange) temperatures on the studied vessel

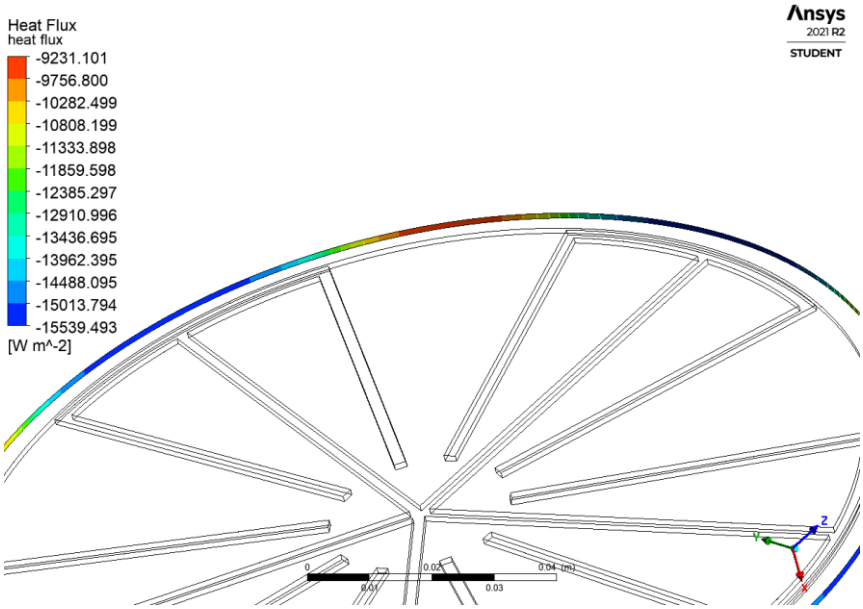

FIGURE 6: Heat removal by cooling

FIG. 6 shows the removal of heat from the metal hydride vessel by cooling around the perimeter of the steel casing. The greatest values of heat dissipation are found in the places of the primary ribs.

IV. CONCLUSION

The goal of the simulation in the ANSYS CFX program was to design an internal heat transfer intensifier that will effectively remove heat from the core of the metal hydride storage vessel to the outer shell, where the storage vessel is cooled by a cooling liquid. The simulation results showed that the designed intensifier achieves optimal values in all areas of investigation.

ACKNOWLEDGEMENTS

This paper was written with the financial support from the VEGA granting agency within the project solutions No. 1/0626/20 and No. 1/0532/22 from the KEGA granting agency within the project solutions No. 012TUKE-4/2022 and with financial support from the granting agency APVV within the Project Solution No. APVV-15-0202, APVV-21-0274 and APVV-20 0205.

REFERENCES

[1] Jose Bellosta von Colbe; Application of hydrides in hydrogen storage and compression: Achievements, outlook and perspectives, International Journal of Hydrogen Energy, 7780-7808, 2019.

[2] Mykhaylo Lototskyy; Metal hydride hydrogen storage tank for fuel cell utility vehicles, International Journal of Hydrogen Energy, 7958-7967, 2020.

[3] Vinod Kumar Sharma; Metal hydrides for energy applications – classification, PCI characterization and simulation, 901-923, Wiley, 2017

[4] Afzal, M. Mane, R. Sharma, P.: Heat transfer techniques in metal hydride hydrogen storage: A review. International Journal of Hydrogen Energy 42, 2017.

[5] Chibani, A. Bougriou, Ch. Merouani, S.: Simulation of hydrogen absorption/desorption on metal hydride LaNi5-H2: Mass and heat transfer. Applied Thermal Engineering 142, 2018.

[6] STN EN 13322-2, Prepravné fľaše na plyny. Navrhovanie a výroba znovuplniteľných oceľových fliaš na plyny. Časť 2: Nehrdzavejúce ocele, 2003

[7] Bocko, Jozef; Lengvarský, Pavol; Huňady, Róbert; Delyová, Ingrid. Simulácia v programe ANSYS. Stojnícka fakulta, Technická Univerzita v Košiciach, 2020.

Design of an Optimized Graphite Electrode Cooling System by using Numerical Simulations

Ivan Mihálik[1*], Tomáš Brestovič[2], Marián Lázár[3], Šimon Hudák[4]

Department of Power Engineering, Faculty of Mechanical Engineering, Technical University of Košice, Slovakia
*Corresponding Author

Received: 03 November 2022/ Revised: 11 November 2022/ Accepted: 19 November 2022/ Published: 30-11-2022

Abstract— *The article deals with the design of optimization of graphite electrode cooling in a plasma reactor. By means of experimentally obtained data during the operation of the plasma reactor, it analyzes the current state of electrode cooling. Based on the measured temperatures at the inlet and outlet of the reactor and on the basis of the calculated flow rate of the cooling medium, it proposes a suitable solution for the optimization of the cooling system in the plasma reactor providing the necessary cooling power by analytical calculations with the use of software support. The proposed solution works on the principle of a water-air type heat exchanger. The verification of this proposal is carried out by numerical simulations using the Ansys CFX software*.

Keywords— CFD simulation, cooling, heat exchanger, plasma reactor.

I. INTRODUCTION

Sufficient cooling is necessary to ensure the long service life of the electrode in the plasma reactor and its proper functioning. The high temperatures reached during operation can cause a high rate of electrode erosion. Heat transfer at the cathode occurs by radiation, convection, conduction and the influence of electron interaction. The cathode is also heated during operation by the electric current that passes through it. As the cathode is one of the elements with the highest temperature in the plasma torch, practically everything that is in contact with it serves as a thermal cooler.

The original cooling system works on the principle of an open cooling circuit. Thus, fresh water is supplied to the cooler using a water service line from the building in which the reactor is located. After heating, the water is then drained into the sewer pipe. Such a cooling system is highly inefficient and results in extremely high consumption of water. For this reason, it is necessary to change the system to a cooling system with a closed water circuit.

II. CURRENT STATE OF THE COOLING SYSTEM

The water cooler is located on the lid of the plasma reactor. It consists of 2 mm welded steel sheets. The dimensions of the water cooler are 200 x 230 mm with a total height of 44 mm. In addition to the water circuit, cooling in the plasma reactor is also provided by a fan. It is located on the frame of the plasma reactor and blows the air around the part of the hollow electrode protruding above the cooler. At the same time, the nitrogen supplied to its upper part serves to cool the electrode. The cooling system is shown in Fig. 1.

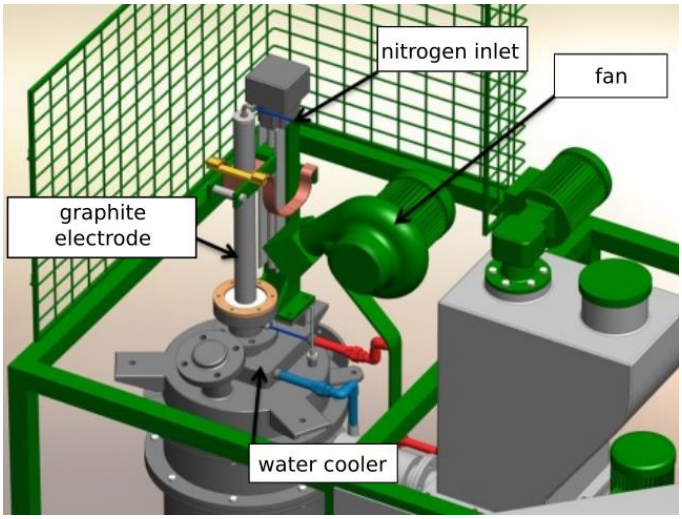

FIGURE 1: Current graphite electrode cooling system

2.1 Measurement of flow and temperatures at the inlet and outlet of the water cooler

To calculate the heat output of the cooler, it was necessary, among other things, to determine the volume flow of the cooling medium and the temperature difference at the inlet and outlet of the medium from the cooler. The required data were obtained by experimental measurement.

The water at the inlet of the reactor was kept at a constant value of 12 °C throughout the duration of the experiment. The temperature of the water at the outlet of the cooler depended on the rising temperature of the reactor. The highest temperature in the plasma reactor was recorded after 132 minutes, when it reached a value of 1 399 °C. The highest measured water value at the outlet of the cooler was 25 °C.

The volumetric flow rate was determined using an Almemo measuring device located in the cooling circuit. Flow values were recorded at 1-minute intervals. Since flow regulation was not necessary during the operation of the reactor, it was maintained at approximately a constant level of $1{,}667 \cdot 10^{-5}$ $m^3 \cdot s^{-1}$ during the duration of the experiment.

2.2 Determination of the thermal performance of the water cooler

The thermal performance of the cooler can be expressed using the equation (1) as the ratio of the change in the amount of heat over a certain time:

$$P_c = \frac{dQ}{d\tau} = \frac{m \cdot c \cdot \Delta t}{\Delta \tau} \quad (W) \tag{1}$$

Where dQ is the elementary amount of heat (J), dτ - the elementary time change (s), m - the mass of the cooling medium (kg), c - the specific heat capacity of the cooling medium ($J \cdot kg^{-1} \cdot K^{-1}$), Δt - temperature difference of the cooling medium between the inlet and outlet of the cooler (K).

Then it holds that:

$$P_c = Q_m \cdot c \cdot \Delta t \quad (W) \tag{2}$$

where Q_m is the mass flow rate of the cooling medium ($kg \cdot s^{-1}$).

The mass flow in equation (2) can be replaced by the volume flow according to equation (3):

$$P_c = Q_v \cdot \rho \cdot c \cdot \Delta t \quad (W) \tag{3}$$

where ρ is the density of the cooling medium ($kg \cdot m^{-3}$).

For the calculation, the mean values of the specific heat capacity and density were considered for the temperature interval t_1 = 12 °C and t_2 = 25 °C. Average specific heat capacity of water $\bar{c}$ = 4183,96 $J \cdot kg^{-1} \cdot K^{-1}$ and average density of water $\bar{\rho}$ = 998,45 $kg \cdot m^{-3}$. Then for the thermal performance P:

$$P = Q_v \cdot \bar{\rho} \cdot \bar{c} \, (t_2 - t_1) \quad (W)$$

$$P = 1{,}667 \cdot 10^{-5} \cdot 998{,}45 \cdot 4183{,}96\ (25 - 12) = 905{,}07\ \text{W} \tag{4}$$

For the new optimized design of the cooling system, a slightly increased cooling power at the level of P_c = 1 kW was considered. The reason for this power increase is to ensure the reliable operation of the reactor with a sufficient power reserve.

III. DETERMINATION OF THE OPTIMIZED COOLING SYSTEM PARAMETERS

The optimized system uses a closed cooling water circuit. Water circuit pipes are cooled by air flow through the fan. It is therefore a design of a heat exchanger based on the principle of water - air.

3.1 Determination of the thermal conductivity coefficient "kL"

The thermal conductivity coefficient depends on the type of heat carrier and on the type of the flow. Its increase can generally be achieved by accelerating the flow of the heat carrier. Its value is also influenced by the layout of the tubes and the air flow around them, as the tubes can be arranged in a row or alternately. The optimization of these parameters was achieved using the SPT-NK software, which uses criterion equations for calculation. This software allows to find an optimal solution without the need for analytical calculations.

The thermal conductivity coefficient k_L for the cylindrical wall can be calculated using the equation (5):

$$k_L = \left(\frac{1}{\alpha_1 \cdot D_1 \cdot \pi} + k_c + \frac{1}{\alpha_2 \cdot D_2 \cdot \pi}\right)^{-1}\ (\text{W} \cdot \text{m}^{-1} \cdot \text{K}^{-1}) \tag{5}$$

The middle term kc of the equation (5) expresses heat transfer by conduction through the pipe wall and has very little influence on the overall thermal conductivity coefficient. It is therefore possible to neglect it.

3.1.1 Heat transfer coefficient on the inside of the pipe α1

It was decided to create a construction of a copper cooler consisting of copper pipes with dimensions of 18x1 mm, while the total length of the pipes was defined as 23 m for the calculation of the heat transfer coefficient inside the pipe. The water flow was provided by a circulating pump, and the speed of the fluid flow through the pipe reached a value of 0,083 m·s^{-1}. The temperature at the inlet to the heat exchanger t_1 was defined as 50 °C and the wall temperature t_S = 26 °C. The temperature at the outlet of the exchanger t_2 was calculated using equation (6):

$$t_2 = t_1 - \frac{P_c}{Q_v \cdot \bar{\rho} \cdot \bar{c}}\ (°\text{C})$$

$$t_2 = 50 - \frac{1000}{1{,}667 \cdot 10^{-5} \cdot 998{,}45 \cdot 4183{,}96} = 35{,}64\ °\text{C} \tag{6}$$

3.1.2 Heat transfer coefficient on the outside of the pipe α2

When calculating the heat transfer coefficient on the outside of the pipe, an alternating layout of pipes was considered. Unlike pipes placed in a row, such a layout can ensure a higher value of the heat transfer coef-ficient. The horizontal distance between the axes of the pipes was defined by the value s_1 = 0,025 m, and the vertical distance s_2 = 0,05253 m.

At air flow rate Q_A = 0,8334 m^3·s^{-1}, the flow velocity was 2,5 m·s^{-1}. The temperature t_3 = 25 °C was determined by measuring the ambient air temperature. Air density ρ_A = 1,185 kg·m^{-3} and specific heat capacity of air c_A = 1 013 J·kg^{-1}·K^{-1} was determined from the tables at temperature t_1 = 25 °C and atmospheric pressure p = 101 325 Pa. The temperature of the pipe wall was defined by the mean temperature of the water in the pipe as t_S = 404 °C. Air temperature t_4 after removing heat from the tubes was determined from equation (7):

$$\Delta t = \frac{P_c}{Q_A \cdot \rho_A \cdot c_A}\ (°\text{C})$$

$$t_4 = t_3 + \frac{P_c}{Q_A \cdot \rho_A \cdot c_A}\ (°\text{C})$$

$$t_4 = 25 + \frac{1000}{0{,}8334 \cdot 1{,}185 \cdot 1013} \cong 26\ °\text{C} \tag{7}$$

The values of the heat transfer coefficients obtained by the SPT-NK software by using the input parameters are shown in the Table 1.

TABLE 1
VALUES OF THE HEAT TRANSFER COEFFICIENTS

	($W \cdot m^{-2} \cdot K^{-1}$)
α_1 - the inside of the pipe	146,17
α_2 - the outside of the pipe	91,28

after substituting into equation (5), the coefficient k_L for the cylindrical wall is equal to:

$$k_L = \left(\frac{1}{146{,}17 \cdot 0{,}016 \cdot \pi} + \frac{1}{91{,}28 \cdot 0{,}018 \cdot \pi}\right)^{-1} = 3{,}0318\ W \cdot m^{-1} \cdot K^{-1} \quad (8)$$

3.2 Determination of the mean logarithmic temperature difference "($\overline{\Delta t}$)"

The equation (8) for calculating the mean logarithmic difference has the form:

$$\Delta t_{LMTD} = \frac{\Delta t_1 - \Delta t_2}{\ln \frac{\Delta t_1}{\Delta t_2}}\ (°C) \quad (9)$$

while it is based on the course of temperatures in the counterflow in Fig. 2.

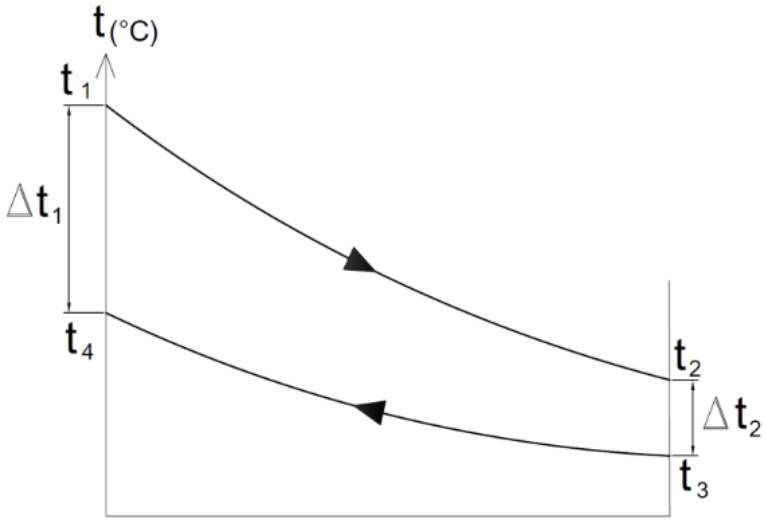

FIGURE 2: Temperature course for counterflow

Then for the temperature differences Δt_1 a Δt_2:

$$\Delta t_1 = t_1 - t_4\ (°C)$$

$$\Delta t_1 = 50 - 26 = 24\ °C \quad (10)$$

$$\Delta t_2 = t_2 - t_3\ (°C)$$

$$\Delta t_2 = 35{,}64 - 25 = 10{,}64\ °C \quad (11)$$

However, since it is a cross arrangement of the heat exchanger, a correction of equation (8) using the correction factor ε is necessary to calculate the mean logarithmic temperature difference. Then applies:

$$\overline{\Delta t} = \varepsilon \cdot \Delta t_{LMTD}\ (°C) \quad (12)$$

To determine the correction factor ε, it is necessary to know the parameters R and P, for which the following applies:

$$R = \left|\frac{t_3 - t_4}{t_1 - t_2}\right| \quad (13)$$

$$R = \left|\frac{25 - 26}{50 - 35{,}64}\right| = 0{,}07$$

$$P = \left|\frac{t_1 - t_2}{t_1 - t_3}\right|$$

$$P = \left|\frac{50 - 35{,}64}{50 - 25}\right| = 0{,}5744 \tag{14}$$

The correction factor ε can then be determined from the Fig. 3 as ε = 0,99.

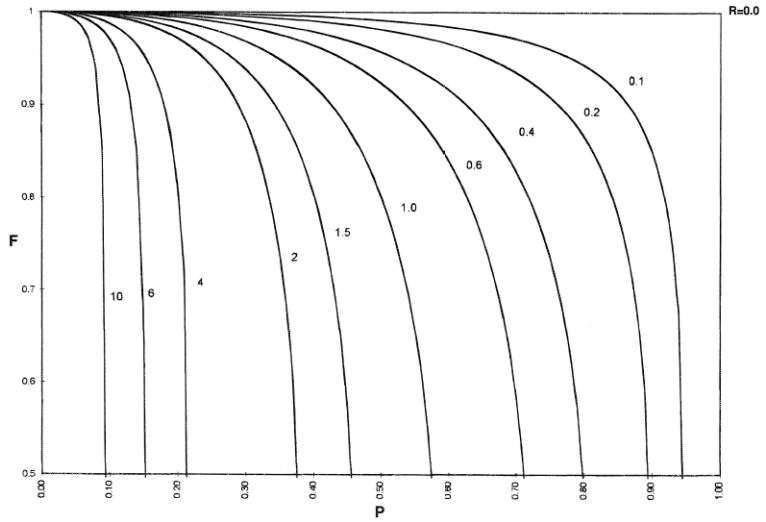

FIGURE 3: Determination of the correction factor

After substituting into equation (11), it holds that:

$$\overline{\Delta t} = 0{,}99 \cdot \frac{24 - 10{,}64}{\ln\frac{24}{10{,}64}} = 16{,}26\ ℃$$

After substituting the thermal conductivity coefficient k_L and the mean logarithmic temperature difference $\overline{\Delta t}$ into equation (14) and subsequent adjustment, the following applies:

$$P_c = k \cdot L \cdot \overline{\Delta t}\ \ (\mathrm{W}) \tag{15}$$

$$L = \frac{P_c}{k \cdot \overline{\Delta t}} = \frac{1000}{3{,}0318 \cdot 16{,}26} = 20{,}29\ \mathrm{m} \tag{16}$$

Where L is the total required length of copper piping for the design of the heat exchanger with the specified cooling performance (m).

IV. NUMERICAL SIMULATION OF AIRFLOW AND HEAT TRANSFER OF AN OPTIMIZED COOLING SYSTEM

The heat exchanger model must be designed in such a way that the air flow velocity reaches a value of at least 2,5 $m \cdot s^{-1}$ in every place of the cooler. A total of 50 tubes were used, each 400 mm long. They are located inside the exchanger chamber in a pipe with a cross-section of 400 x 355 mm and a total length of 300 mm. 49 standardized arcs were used to connect the individual pipes to each other. Since these arcs are not located inside the exchanger chamber, they ensure heat transfer only through natural convection. For this reason, they were not included in the total required pipe length. The model of the designed exchanger chamber in Fig. 4 was created using SolidWorks CAD software.

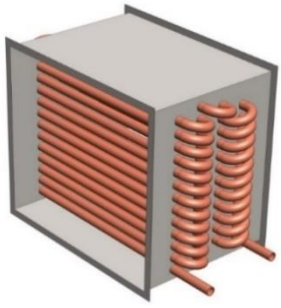

FIGURE 4: Exchanger chamber

Before the simulation of heat transfer, it was first necessary to verify on the given model whether the estimated air flow Q_A = 0,8334 $m^3 \cdot s^{-1}$ is satisfactory for the given layout of pipes. The FloXpress add-on in the SolidWorks software was used to verify this assumption. The result of the simulation are graphic contours in Figure 5 a) depicting the air speed. In Fig. 5 b) the scale is bounded by the value 2,5 $m \cdot s^{-1}$.

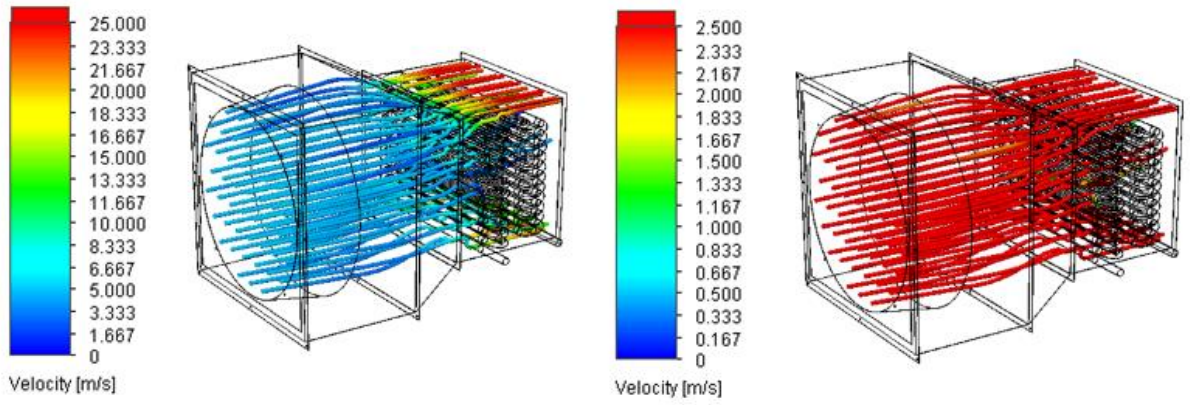

a) Airflow – unbounded scale **b) Airflow – scale bounded by 2,5**

FIGURE 5: Airflow velocity in the heat exchanger

It is clear from the Figure 5 b) that the air reaches the required air flow speed in almost every place of the exchanger. The air flow and the layout of the tubes can therefore be considered satisfactory.

The Ansys CFX program was used for heat transfer simulation. At the inlet to the exchanger, a temperature of 50 °C and a water flow rate of 0,01667 $kg \cdot s^{-1}$ were defined, while laminar flow was considered. A relative pressure of 0 Pa was defined at the outlet of the exchanger. The heat transfer coefficient on the surface of the tubes in the inner part of the exchanger for forced convection has the value α_2 = 91,28 $W \cdot m^{-2} \cdot K^{-1}$. The heat transfer coefficient on the surface of the arcs in the outer part of the exchanger for natural convection was defined as a function by using the SPT-VK software.

V. EVALUATION

The simulation results confirmed that the proposed heat exchanger solution is satisfactory. The Fig. 6 shows the temperatures on the surface of the heat exchanger tubes.

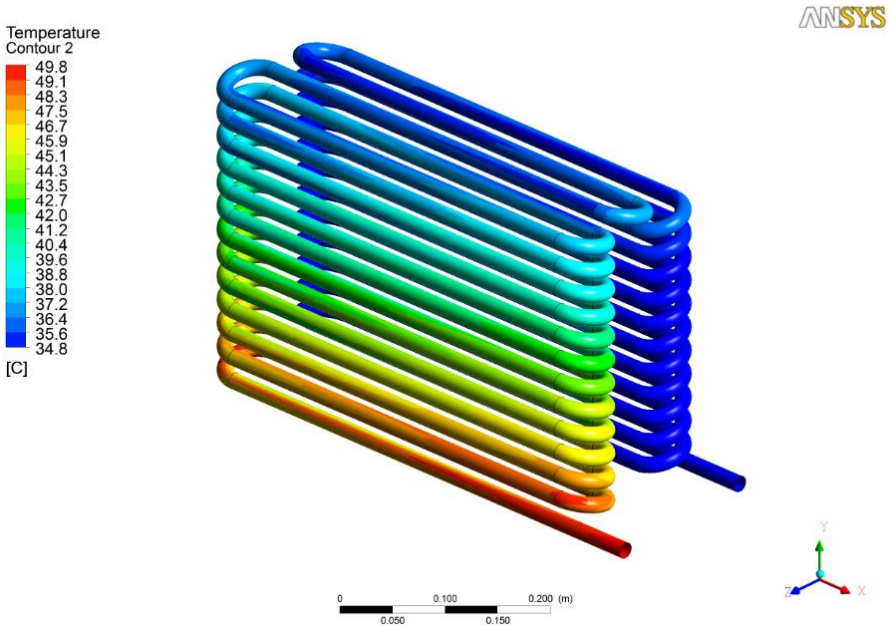

FIGURE 6: Temperature contours of the heat exchanger

The temperature of the water in the pipeline at the outlet of the heat exchanger reaches 30,5 °C. The heat flow removed by the flowing air reached a value of almost 1200 W. The increase in cooling power compared to the proposed 1000 W was probably caused by the neglect of the length of the pipe bends when determining the total length.

VI. CONCLUSION

The resulting design of the air-water exchanger provides a cooling capacity approximately 20% higher than the required 1 kW. Due to the relatively robust construction of this solution, it would therefore be possible to shorten the total length of the exchanger tubes, which would allow more compact dimensions of the device to be achieved. Minimizing the dimensions could also be achieved by using a heat exchanger equipped with different ribbed surfaces.

ACKNOWLEDGEMENTS

This paper was written with the financial support from the VEGA granting agency within the project solutions No. 1/0626/20 and No. 1/0532/22 from the KEGA granting agency within the project solutions No. 012TUKE-4/2022 and with financial support from the granting agency APVV within the Project Solution No. APVV-15-0202, APVV-21-0274 and APVV-20-0205.

REFERENCES

[1] Balaji, C., Srinivasan, B., Gedupudi, S. (2020). Chapter 7 - Heat exchangers. In: Heat Transfer Engineering, p. 199 – 231. ISBN: 978-0-12-818503-2

[2] Zhukov, M. F. – Zasypkin, I. M. (2007). Thermal Plasma Torches. ISBN: 978-1-904602-02-6

[3] Galimore, S. (1998). Operation of a High-Pressure Uncooled Plasma Torch with Hydrocarbon Feedstocks.

[4] Lendhard, R., Kaduchová, K., Jandačka, J. (2014). Numerical simulation of indirectly heated hot water heater. *Advanced Materials Research*, vol. 875-877, p. 1693-1697. https://doi.org/10.4028/www.scientific.net/AMR.875-877.1693.

The Process of Heat Exchange in A Piece Batch

Romana Dobáková[1*], Ľubomíra Kmeťová[2], Lukáš Tóth[3]

Department of Power Engineering, Faculty of Mechanical Engineering, Technical University of Košice, Slovakia
*Corresponding Author

Received: 02 November 2022/ Revised: 10 November 2022/ Accepted: 17 November 2022/ Published: 30-11-2022

Abstract— *The most important phenomenon in technical practice, which affects the thermal regime of industrial aggregates, includes, among others, the heat exchange process, which is primarily characterized by the heat trans-fer coefficient. The article analyses the influence of the grain size of the batch and the flow rate of the gaseous heat-carrying medium on the heat transfer coefficient during heating of the batch to the required temperature as a function of time. The experimental measurement was carried out on shaft furnace models.*

Keywords— Industrial Aggregates, The Batch, Heat Transfer, Heat Transfer Coefficient.

I. INTRODUCTION

Metallurgical furnaces are complex mechanized and automated devices. The processes that take place in them are equally complex.

A charge is placed in the working space of the furnace and then the thermal process is started. The essence of this process is heating to a temperature that leads to a change in the state of the batch or to a temperature sufficient for its further processing. To increase the temperature in industrial furnaces, it is necessary to bring heat into the working space of the furnace, or to develop heat directly in the furnace and transfer it to the batch. The thermal regime of these industrial aggregates is very complex, therefore it is necessary to pay due attention to it.

II. HEAT EXCHANGE PROCESS IN BATCH

The exchange of heat in the layer of piece batch in the form of ground granulate of non-homogenized shape of grains of different granularity formed by heat-resistant material in shaft furnaces and similar furnace aggregates is ensured by direct contact of the gaseous heat-carrying medium with the charge. The heat ex-change process itself is ensured by radiation, convection as well as heat conduction in the batch itself. The radiant component is represented to a lesser extent and in practice is mainly used at high batch temperatures. Heat exchange by conduction occurs between the individual parts of the batch and represents a negligible part compared to the heat exchange between the flowing gaseous medium and the particles of the solid substance.

The intensity of heat exchange between two substances, which are most often a gas and a solid, is repre-sented by the heat transfer coefficient. Its value depends on several factors such as grain size and tempera-ture of the batch, temperature and speed of the flowing gas medium, power of the furnace unit, etc.

III. CHARACTERISTICS AFFECTING THE HEAT EXCHANGE PROCESS IN THE BATCH

The examined batch represented an immobile cohesive layer, the particles of which were deposited close to each other, at rest with respect to each other as well as to the walls of the working environment of the furnace unit in which they were deposited. The gas, whose flow was uneven, passed through the layer deposited in this way.

For experimental purposes, crushed fireclay of different grain size was used as a feed, and heated air of a known temperature and volume was used as a gas medium. Flue gas from the process of burning natural gas with air was used to heat the gas medium.

The basic parameters that characterize the cohesive layer include:

- spacing,
- bulk density,
- specific surface,
- characteristic size and shape of solid particles.

The spacing of the layer of particles is a dimensionless quantity determined by the ratio of the volumes of free spaces and the total volume of the layer [2]:

$$\varepsilon = \frac{V_c - V_m}{V_c} \text{ (m}^2\text{·kg}^{-1}\text{)} \quad (1)$$

where V_c is the total volume of the batch layer (m^3), V_m – the volume of the batch particles (m^3).

The spacing depends on several parameters, which can include geometric parameters given by the ratio of the determining dimensions of the layer and particles, the shape of the particles, the granulometric composition of the layer, etc. The method of creating the layer, or method of depositing particles in a layer [2].

Bulk density is also an important parameter characterizing the properties of granular material, which depends on the density of the batch and its spacing. It is defined as the ratio of the total weight of the batch to the total volume that the batch occupies:

$$\rho_S = \frac{M_m}{V} \text{ (kg·m}^{-3}\text{)} \quad (2)$$

where M_m is the total weight of the batch (kg), V – the total volume of the batch (m^3),

respectively in the case of dispersion systems, a solid particle – gas relationship applies:

$$\rho_S = \rho_m \cdot (1 - \varepsilon) \text{ (kg·m}^{-3}\text{)} \quad (3)$$

where ρ_m is batch density (kg·m^{-3}).

The specific surface area of the particles affects the amount of thermal energy that the batch is able to receive from the heat-carrying medium, and it can be related to the weight of the considered amount of particles or their volume.

The mass specific surface is given by the ratio of the surface of the particles in the batch to the weight of the particles of the batch:

$$a_m = \frac{S}{M_m} \text{ (m}^2\text{·kg}^{-1}\text{)} \quad (4)$$

where S is the surface of the particles in the batch (m^2), M_m – weight of the particles (kg),

respectively the specific surface area related to the volume is given by the relation:

$$a_V = \frac{S}{V} \text{ (m}^2\text{·m}^{-3}\text{)} \quad (5)$$

The efficiency of industrial furnaces is also linked to the conditions of the gas medium flow. Many factors depend on the nature of the flow, which can include the intensity of heat exchange in the working space, the distribution of temperature and pressure along the layer of the batch, as well as resistance to flow and spacing [4].

The gas flow through the cohesive layer is non-uniform and can be considered as the movement of the medium in the channels that are formed between the particles of the solid charge and between the particles and the wall of the working space of the furnace. As the compaction of the batch increases, the channels for the flow of the heat-carrying substance in the volume of the material become smaller, which leads to an increase in pressure losses and redirection of the gas flow to areas with less compaction, or to the walls of the aggregate. Compacting the batch will improve the contact of the individual grains but will reduce the efficiency of the entire heating process.

IV. DESCRIPTION OF THE EXPERIMENT

The experimental measurement required to determine the heat transfer coefficient was carried out on a reduced model of the shaft furnace (fig. 1), the basic parameters of which are listed in tab. 1. At the bottom of the furnace model there was a stepped grate on which the batch was stored. During the experiment, the particle size of the batch changed as well as the air flow. There was a pipe under the grate, with the help of which heated air was blown into the working space of the furnace. Before the

measurement itself, it was necessary to stabilize the temperature of the batch, which was achieved by blowing in air of ambient temperature. During the experiment, the temperature of the batch material and the temperature of the flowing air were measured.

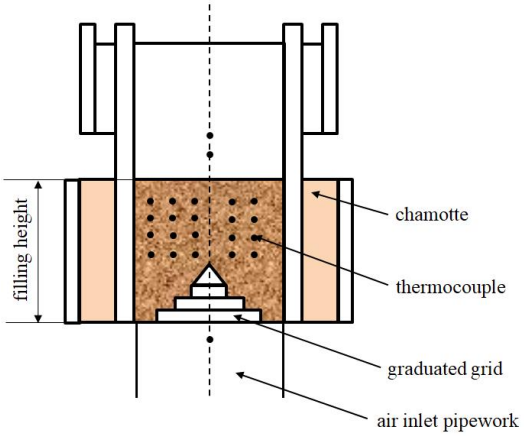

FIGURE 1: Furnace model with the distribution of thermocouples

Air flow was measured using a gas meter and its pressure using U-tube pressure gauges. The temperature of the charge and air was measured by touch thermocouples type K (NiCr-Ni).

TABLE 1
BASIC PARAMETERS OF THE FURNACE MODEL

height of the furnace model (mm)	856		
Inner pipe diameter (mm)	110		
Height of batch (mm)	488		
gas medium	air		
Batch	crushed fireclay		
Batch density (kg·m^{-3})	1900		
the volume of the furnace at the height of the batch (m^3)	0.046		
batch granularity (mm)	8-Apr	10-Aug	12-Oct
Spacing of batch (1)	0.55	0.61	0.623
Air flow (m^3·h^{-1})	56.3	78	

V. DETERMINATION OF THE HEAT TRANSFER COEFFICIENT

When determining the heat transfer coefficient, balance equations were used, by comparing which a relationship was obtained for the expression of the heat transfer coefficient related to the volume of the furnace model:

$$\alpha_V = \frac{m_m \cdot c_m \cdot (t_m'' - t_m')}{V_C \cdot \Delta t_{LS} \cdot \tau} \text{ (W·m}^{-3}\text{·K}^{-1}\text{)} \quad (6)$$

where m_m is the batch weight (kg), c_m - average specific heat capacity of the batch(J·kg^{-1}·K^{-1}), t_m' - temperature of the batch at the inlet (°C), t_m'' - temperature of the batch at the outlet (°C), V_C - volume of the shaft furnace model (m^3), τ - time (s), Δt_{LS}- mean logarithmic temperature difference (K), for which the relation applies:

$$\Delta t_{LS} = \frac{\Delta t' - \Delta t''}{\ln \frac{\Delta t'}{\Delta t''}} \text{ (K)} \quad (7)$$

where $t_{vz}' - t_m'' = \Delta t'$ is the temperature difference between the air and the batch at the inlet to the model and $t_{vz}'' - t_m' = \Delta t''$ temperature difference of the air and the charge at the outlet of the model.

In fig. 2, 3 shows the course of the heat transfer coefficient as a function of time at three different particle sizes for air flows of 56.3 m^3·h^{-1} and 78 m^3·h^{-1}.

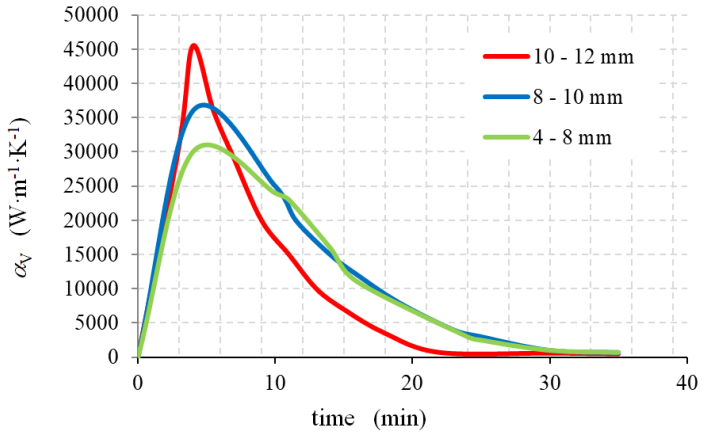

FIGURE 2: The course of the heat transfer coefficient as a function of time at three different grain sizes in the air flow 56.3 m^3·h^{-1}

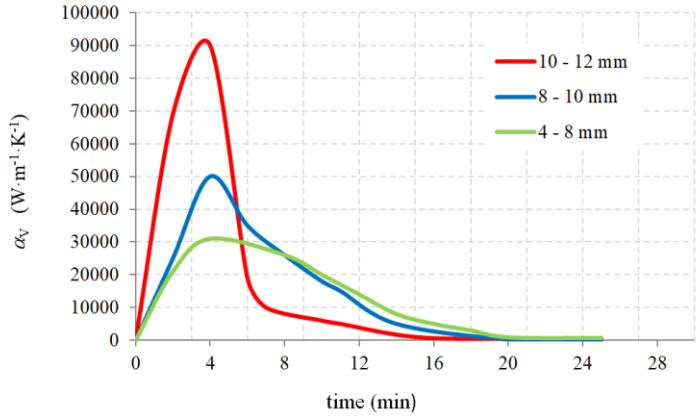

FIGURE 3: The course of the heat transfer coefficient as a function of time at three different grain sizes in the air flow 78 m^3·h^{-1}

From the graphical dependencies shown in fig. 2 and 3 clearly shows that the smaller the particle size of the batch, the lower the heat transfer coefficient between the batch and the heated air. Since the heat transfer coefficient depends on the heat exchange surface of the batch, it can be observed from the dependence that the batch with a larger heat exchange surface is able to receive more heat than the batch with smaller grain size in the same period of time, which means that the batch heated up to the required temperature earlier than in the case of small grain size.

In fig. 4, 5 show the courses of the heat transfer coefficient as a function of time at two different flow rates for batch grain sizes 10 – 12 mm and 4 – 8 mm.

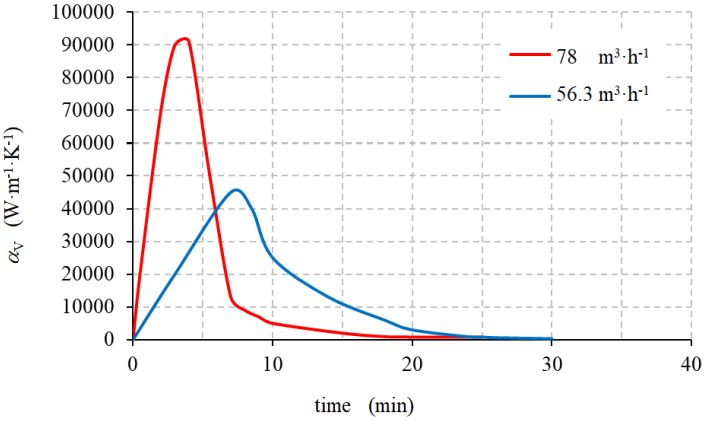

FIGURE 4: The course of the heat transfer coefficient as a function of time at a particle size of 10-12 mm at air flows 56.3 and 78 m^3·h^{-1}

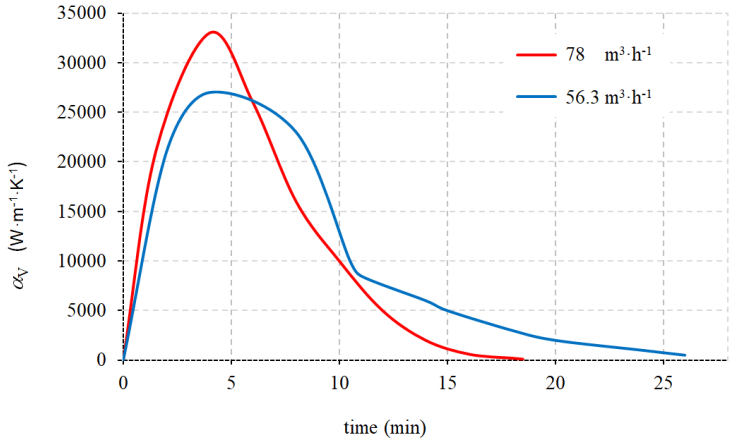

FIGURE 5: The course of the heat transfer coefficient as a function of time at batch granularity of 4 – 8 mm at air flows of 56.3 a 78 m^3·h^{-1}

The speed of the air flow depends on the flow rate. When comparing the dependence curves of the heat transfer coefficient in fig. 4, 5, which describe the development of the heat transfer coefficient at two different air flows, it clearly follows that the higher the air flow, the higher the heat transfer coefficient and the time required for heating the batch is shortened. At a higher flow rate, a larger amount of heated air enters the furnace, which transfers a larger amount of heat to the batch, and thus shortens the time required for its heating.

VI. CONCLUSION

The The value of the heat transfer coefficient from the flowing air to the batch depends on several factors. The grain size of the batch, the uniformity of the distribution of the batch, the inlet temperature of the flowing air as well as the amount of the heat-carrying medium flowing through the batch play a role.

As the particle size of the batch increased, the air flow through the batch also increased, which caused a faster and more homogeneous overheating of the material. In order to achieve more optimal heat transfer at lower grain sizes, it is necessary to ensure a higher air flow in order to achieve comparable heat transfer results between the air and the batch.

In order to increase the overall efficiency of industrial aggregates and reduce the costs associated with the operation of such devices, it is necessary to ensure optimal conditions for the transfer of heat from the heat-carrying medium to the material of the batch, which will also reduce the energy demand of the process and the time required for melting or heating the material to the required technological temperatures.

ACKNOWLEDGEMENTS

This paper was written with the financial support from the VEGA granting agency within the project solutions No. 1/0626/20 and No. 1/0532/22 from the KEGA granting agency within the project solutions No. 012TUKE-4/2022 and with financial support from the granting agency APVV within the Project Solution No. APVV-15-0202, APVV-21-0274 and APVV-20-0205.

REFERENCES

[1] Repášová, M., Míček, M. (1992). Tepelné režímy. VŠT Košice.

[2] Rédr, M., Príhoda, M. (1973). Základy tepelenej techniky. SNTL Praha.

[3] Stopar, K., Kovačič, M., Kitak, P., Pihler, J. (2014). Electric-arc-furnace productivity optimization, Materiali in technologije/Materials and technology. 48 (1), p. 3–7.

[4] Kalčík, J., Sýkora, K. (1973). Technická termomechanika. Academia Praha.

[5] Beňo, J., Vontorová, J., Matějka, V., Gál, K. (2014). Evaluation of the thermal resistance of selected bentonite binders, Mater. Tehnol., 49 (3), p. 465–469.

Methanization of Lemna Minor for the Purpose of obtaining Hydrogen

Lukáš Tóth[1*], Marián Lázár[2], Filip Duda[3]

Department of Power Engineering, Faculty of Mechanical Engineering, Technical University of Košice, Slovakia
*Corresponding Author

Received: 04 November 2022/ Revised: 14 November 2022/ Accepted: 21 November 2022/ Published: 30-11-2022

Abstract— *The article discusses the theoretical possibilities of using biomass produced on open water bodies by growing the Lemna minor plant for hydrogen production. The process of obtaining hydrogen is solved primarily in two stages, including the methanization of biomass and the subsequent transformation of methane into hydrogen and carbon dioxide. It deals with current technologies of methane oxidation to form hydrogen using water vapor, such as WGSR, SMR, MPS and PSMR technologies. It indicates various methods of purifying hydrogen from unwanted elements with their subsequent applicability in small local hydrogen production plants in decentralized hydrogen economy.*

Keywords— hydrogen, Lemna minor, methane, biomass.

I. INTRODUCTION

Globally increasing requirements for obtaining hydrogen using technologies that do not use fossil resources for their operation nor for the production of hydrogen, are increasing with the rising prices of fossil sources and gradual reduction of the number of their abundant deposits. The production of green hydrogen by the means of the electrolytic decomposition of water using renewable sources of energy currently faces obstacles with the lack of renewable sources of electric energy. One of the ways to decrease the dependence on fossil sources during the hydrogen production process is the use of organic biomass, the processing of which produces the so-called blue hydrogen. However, the use of biomass also encounters problems with land, when large volumes of arable land intended for growing food are occupied at the expense of the cultivation of biomass that can be used for energy. This problem is solved by growing biomass on water bodies. The advantage of producing biomass on open water surfaces is the reduction of arable land required for the cultivation of energy recoverable biomass. Another advantage is the increase of yields due to the faster growth of aquatic biomass compared to its terrestrial equivalent. Lemna minor is one of the smallest and fastest-growing flowering plants on the earth. It´s an extremely reduced floating freshwater plant. The growth rate of Lemna minor in the wastewater in an open uncontrolled environment is at the level of 29 $g \cdot m^{-2} \cdot day^{-1}$, as it is dry biomass, which corresponds to 104 $t \cdot ha^{-1} \cdot year^{-1}$. During experiments with new types of fast-growing biomass, such as sun hemp (Crotalaria juncea L.), yields were achieved only at the level of 11 $t \cdot ha^{-1} \cdot year^{-1}$. [2] In the case of fast-growing trees such as willow, the yield can be in the range of 16 – 17 $t \cdot ha^{-1} \cdot year^{-1}$ and in the case of poplar in the range of 18 – 16 $t \cdot ha^{-1} \cdot year^{-1}$. [3] The use of fast-growing herbs such as bamboo can represent of the possibilities of fast and efficient biomass cultivation for energy purposes, but even in this case there are limitations caused by bamboo's requirements for growth conditions. In ideal conditions for growth in an uncontrolled environment, the bamboo reached a maximum yield of 47 $t \cdot ha^{-1} \cdot year^{-1}$. [4]

II. ORGANIC DECOMPOSITION OF LEMNA MINOR INTO METHANE

When producing hydrogen from organic biomass it is possible to use several methods of its processing. Among the simplest methods of processing biomass is the thermal decomposition of organic substances with the simultaneous production of synthesis gas, oils, ash, or solid residues. The thermal recovery process of Lemna minor produces large amounts of carbon dioxide at the expense of the production of hydrogen, carbon monoxide and methane. This problem is caused by the presence of a high proportion of oxygen in the basic biomass, which results in a high production of carbon dioxide, as shown in Fig. 1 from the research of N. Muradov et al.

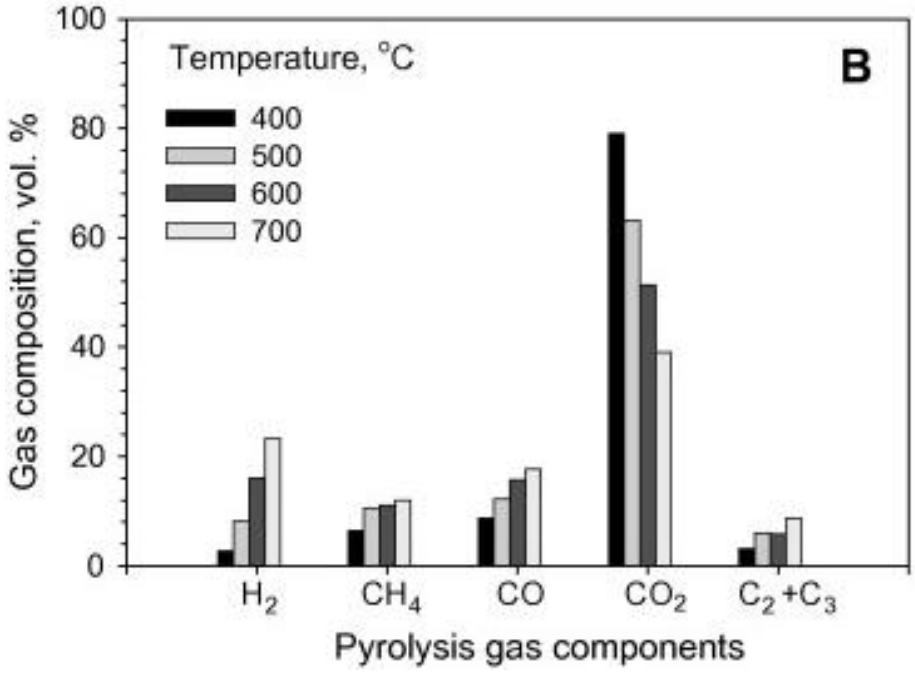

FIGURE 1: Composition of pyrolysis gas produced by Lemna minor pyrolysis depending on pyrolysis temperature at Ar flow rate 60 ml·min^{-1} [5]

One of the variants in which it is possible to increase the yield of hydrogen obtained from Lemna minor biomass is its conversion into methane using methanogenic organisms. By subsequent technological treatment of methane, it is possible to obtain hydrogen to produce carbon dioxide. For the process of converting Lemna minor into methane, it is necessary to carry out the initial pre-treatment of the biomass to increase the efficiency of its recovery. The basis of the pre-treatment is drying and grinding of biomass, which improves the access of substances in the following processes into the organic structure and increases the efficiency of the processes. Grinding is followed by a hydrolysis process, during which the polymeric organic substances (polysaccharides, fats, proteins) with the help of aerobic bacteria are broken down into monomers – alcohols and fatty acids, releasing hydrogen (H_2) and carbon dioxide (CO_2). The produced gases can be captured and added to the treated biogas to increase the yield of hydrogen from the overall process.

After hydrolysis, the treated biomass is transferred to the reactor, where the initial preparation for the direct production of biogas takes place. The first step is acidogenesis, during which the residual oxygen in the air is consumed. An anaerobic environment is created, and higher organic acids are formed. This transformation is carried out by facultative anaerobic microorganisms, which are capable of existing in both environments. During the following process of acetogenesis, higher organic acids and alcohols are converted into acetic acid H_2 and CO_2. The final phase of the entire fermentation process is methanogenesis. It takes place in an environment without access to air and the decomposition of acetic acid into methane CH_4 and CO_2 occurs. Hydrogenotrophic bacteria create methane from H_2 a CO_2 that are dissolved in water. [6] The yield of a mixture of hydrogen and methane can reach the level of 33 mol·kg^{-1} when appropriate procedures are used and if additional equipment is used, the total yield can rise to the level of 38,76 mol·kg^{-1}, as stated by K. Manpreet et al. [7]

III. OBTAINING H_2 FROM BIOGAS RICH IN CH_4

To obtain hydrogen from biogas rich in methane, its technological treatment is necessary. For the purposes of technological treatment of biogas, it is advisable to use systems in which methane is converted by merging with water vapor into hydrogen and carbon dioxide. Such devices include, for example, steam reformers (SMR), in which methane is combined with water vapor according to the equation (1):

$$\mathrm{CH_4 + H_2O \leftrightarrow CO + 3H_2}\ \Delta H_{\mathrm{SR}} = 206\ \mathrm{kJ \cdot mol^{-1}} \quad (1)$$

Subsequently, the gas is treated using WGS reactors, in which carbon monoxide is combined with water vapor in the presence of catalysts according to the equation (2):

$$\mathrm{CO + H_2O \leftrightarrow CO_2 + H_2}\ \Delta H_{\mathrm{WGSR}} = -41\ \mathrm{kJ \cdot mol^{-1}} \quad (2)$$

In addition to changing the ratio of individual incoming components, temperature also has a significant effect on the efficiency of the conversion of carbon monoxide into hydrogen. As was proven in the study created at the Ohio State University, under the leadership of prof. Liang-Shih Fan, in the case of high-temperature conversion, there are significant changes in the efficiency of the whole process by changing the temperature. An increasing tendency to increase CO conversion efficiency can be observed with increasing temperature in the reaction chamber, while the break occurs in the critical temperature region (550-650 °C), after which a gradual decrease in efficiency occurs (Fig. 2). In the case of atmospheric pressure and steam:CO mixing ratio, the conversion increases from 45,8 % at 450 °C to 83,2 % at 600 °C. Subsequently a decrease occurs and at 800 °C the conversion efficiency is at the level of 69,4 %. This phenomenon occurs as result of a decrease in the equilibrium constant, [3] which decreases with increasing temperature. The increase in conversion value can be observed with the increasing steam:CO ratio. While at a 1:1 steam-carbon dioxide mixing ratio and a temperature of 650 °C, the conversion efficiency is 63,5 %, in the case of 2:1 ratio the efficiency reaches a value of 71,6 % and at 3:1 ratio a value of 80,28 %.

$$K_{WGS}=\frac{[CO_2][H_2]}{[CO][H_2O]}=812{,}9-\frac{6{,}628e+5}{T}+\frac{1{,}001e+8}{T^2} \quad (3)$$

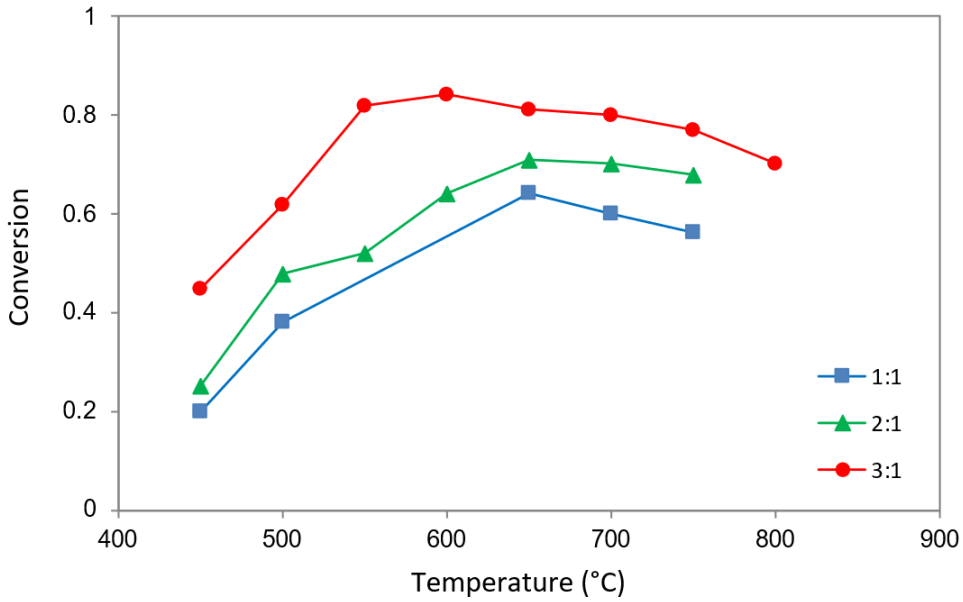

FIGURE 2: Effect of reaction temperature on CO conversion at 0 kPa pressure

Another option that can be used, is the microwave plasma sources (MPS) method, in which methane is combined with water vapor at high temperatures, just like in SMR processes. However, in this case, unlike SMR processes where catalysts are needed, the plasma supplies the necessary energy and free radicals to the process of combining the input raw materials to form H_2 and CO_2 in one step. High energy electrons generated by nonthermal plasma speed up chemical processes leading to the conversion of the methane produced by Lemna minor into hydrogen and carbon dioxide. Significant advantages of nonthermal plasma are its high reactivity and low energy consumption while being able to operate in the low temperature range. Catalysts are usually required in nonthermal plasma to speed up the conversion process. In the area of the discharge, the nonthermal plasma is internally heterogeneous, which leads to a reduction of the reaction surface. As a result, the conversion rates and permeability are low. [7]

Another option for methane valorisation by converting it into hydrogen and carbon dioxide is the plasma steam methane reforming (PSMR) process. During this process, unlike MPS, catalysts are not required for the reaction of methane with water vapor, which results in hydrogen and carbon dioxide. The advantage of microwave plasma is the absence of catalysts, in which clogging occurs during the process of converting methane to hydrogen. Due to clogging of the catalysts, the efficiency of the entire process decreases, and the costs associated with their replacement are increasing. In the paper Plasma steam methane reforming (PSMR) using a microwave torch for commercial-scale distributed hydrogen production, Olugbenga Akande et al. described the process, in which more than 90% conversion of methane to hydrogen and carbon dioxide occurs. In some cases, the over-all conversion efficiency exceeded 99 %.

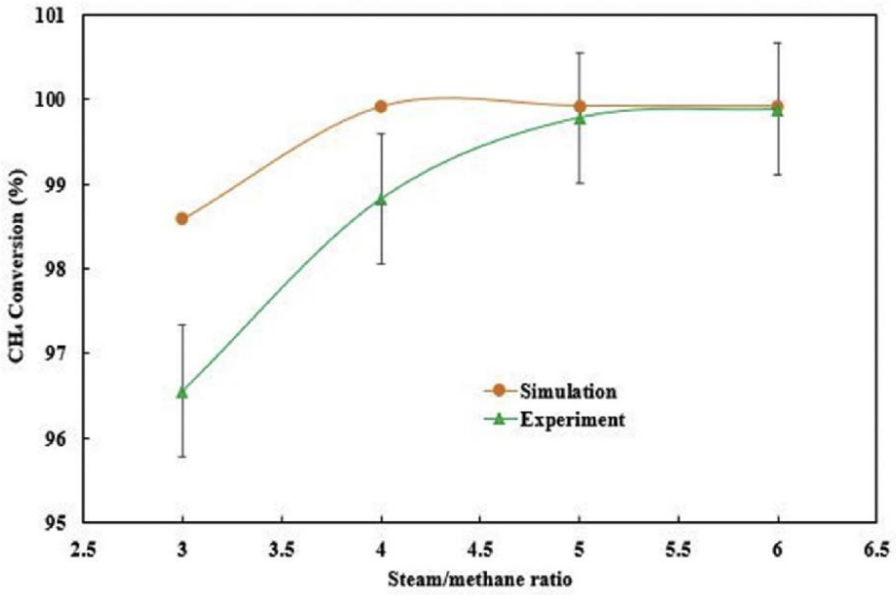

FIGURE 3: Methane Conversion as a function of Steam/Methane Ratio [8]

IV. SEPARATION OF HYDROGEN FROM BINARY MIXTURE OF H_2 AND CO_2

One of the most used methods for the separation of hydrogen from the mixture of gases is the PSA process. It is a process of separating hydrogen from the remaining components using pressure fluctuations in the storage tank (Pressure Swing Adsorption – PSA). The PSA process consists of adsorption unit, in which pressure changes occur and, together with the use of a bed of solid adsorbent, the separation of impurities from the hydrogen stream occurs. The result of this process is a high-purity high-pressure hydrogen and a low-pressure mixture of the remaining gas components containing impurities and part of the hydrogen. The adsorbent beds are regenerated by depressurization and flushing. Part of the hydrogen (up to 20%) can be lost in the waste gas. Adsorption technology during pressure fluctuations is based on the physical binding of gas molecules to the adsorption material. The force acting between the gas molecules and the adsorption material depends on the gas component, the type of adsorption material, the partial pressure of the gas component and the operating temperature. The separation effect is based on the differences in binding forces to the adsorbent material. Highly volatile, low-polarity components such as hydrogen are practically non-adsorbable, unlike molecules such as nitrogen, carbon monoxide, carbon dioxide, hydrocarbon derivatives, and water vapor. Consequently, these impurities can be adsorbed from the hydrogen-rich gas stream. With this method, highly pure hydrogen is obtained. The pressure swing adsorption process works essentially at a constant temperature. It uses the effect of alternating pressure and partial pressure to carry out adsorption and desorption. Due to the absence of cooling and heating devices, which are not necessary in a constant temperature process, the entire process of one cycle can take place in the range of minutes.

In addition to PSA methods, there are also membrane methods in which hydrogen is separated from the remaining components of the gas using a semi-permeable membrane that enables the hydrogen molecules to pass. However, bigger molecules are unable to pass through the membrane. There are generally two classes of membranes for production and purification of hydrogen, both of which are organic: dense phase metals and metal alloys and porous ceramic membranes. Porous ceramic membranes are commonly prepared by sol-gel or hydrothermal methods and have high stability and durability in high-temperature, harsh, polluted and hydrothermal environments.

Membrane systems do not contain any moving parts or switching valves and achieve potentially very high reliability. The main threat are components in the gas (such as aromatic substances) that attack the membranes, or liquids that clog them. The membranes are produced in relatively small modules. For a larger capacity of the device, more modules connected in parallel are added to increase the area of the membranes. Costs increase linearly with capacity, making them more competitive at lower gas capacities being processed. [9]

Many other methods such as cryogenic freezing processes or the use of metal-hydride alloys for hydrogen separation currently represent an expensive or energy-intensive solution for use in decentralized hydrogen production in small local operations.

V. CONCLUSION

Current state of hydrogen production from renewable sources is not currently sufficient for the full competitiveness of green or blue hydrogen against grey hydrogen. The possibilities of producing blue hydrogen using fast-growing biomass appear to be promising in the near future. As proven by the research at the beginning of this article, fast-growing aquatic plants, primarily Lemna family, represent non-negligible source of biomass for the production of the blue hydrogen. Their yields significantly exceed those of terrestrial crops grown for energy purposes. However, the technology of biomass valorisation during the process of hydrogen production from water biomass must take place in less conventional ways due to the high proportion of oxygen in the feed. The consequence of this high proportion is an unacceptable proportion of carbon dioxide during thermal processing of biomass. The possibilities of valorising biomass through its transformation into methane with the use of methanogenic bacteria represent the possibility of increasing the yield of hydrogen compared to thermal decomposition. The subsequent processing of methane using conventional treatment methods, such as SMR and WGSR or new MPS and PSMR methods represents a good basis for improving hydrogen yield. After the subsequent treatment of hydrogen necessary to increase its purity, either by using membrane purification or the PSA process, it is possible to obtain more competitive blue hydrogen compared to grey hydrogen. The processes of hydrogen production from aquatic biomass could enable its decentralization into smaller local enterprises and thereby improve the availability of this fuel for ordinary users.

ACKNOWLEDGEMENTS

This paper was written with the financial support from the VEGA granting agency within the project solutions No. 1/0626/20 and No. 1/0532/22 from the KEGA granting agency within the project solutions No. 012TUKE-4/2022 and with financial support from the granting agency APVV within the Project Solution No. APVV-15-0202, APVV-21-0274 and APVV-20-0205.

REFERENCES

[1] Kaur, M., Srikanth, S., Kumar, M., Sachdeva, S., Puri, S.K.: An integrated approach for efficient conversion of Lemna minor to biogas. Energy Conversion and Management, 180 (2019), p. 25 – 35.

[2] Parenti, A., Cappelli, G., Zegada-Lizarazu, W., Sastre, C.M., Christou, M., Monti, A., Ginaldi, F.: SunnGro: A new crop model for the simulation of sunn hemp (Crotalaria juncea L.) grown under alternative management practices. Biomass and Bioenergy, 146 (2021), DIO:10.1016/j.biombioe.2021.105975.

[3] Teodorescu, T.I., Labresque, M.: Field performance and biomass production of 12 willow and poplar clones in short-rotation coppice in southern Quebec (Canada). Biomass and Bioenergy, 29 (1) (2005), p. 1 – 9.

[4] Truong, A.H., Le, T.M.A.: Overview of bamboo biomass for energy production. (2014).

[5] Muradov, N.,Fidalgo, B., Gujar, A.C., T-Raissi, A.: Pyrolysis of fast-growing aquatic biomass – Lemna minor (duckweed): Characterization of pyrolysis products. Bioresource Technology, 101 (2010). p. 8424 – 8428.

[6] https://energoportal.org/index.php?option=com_content&view=article&id=318&Itemid=432.

[7] Adwek, G., Boxiong, S., Michael, C., Yaolin, W., Dongrui, K., Chunfei, W., Xin, W.: A Review of NonthermalPlasma Technology: a novel solution for CO2 conversion andutilization. Renewable and Sustainable Energy Reviews, 135 (2021), DOI:10.1016/j.rser.2020.109702.

[8] Akande, O., Lee, B.: Plasma steam methane reforming (PSMR) using a microwave torch for commercial-scale distributed hydrogen production. International Journal of Hydrogen Enegry, 47(5) (2021) DOI:10.1016/j.ijhydene.2021.10.258

[9] Speight, J.G.: Heavy Oil Recovery and Upgrading, Chapter 15 - Hydrogen Production. Gulf Professional Publishing, (2019), p. 657-697, ISBN: 978-0-12-813025-4, DOI:10.1016/C2016-0-04682-X.

AD Publications
Sector-3, MP Nagar, Bikaner,
Rajasthan, India
www.adpublications.org, info@adpublications.org